The Astronomical Journal, 162:74 (30pp), 2021 August https://doi.org/10.3847/1538-3881/abfdb7

Investigation of the Origins of Comets as Revealed through Infrared High-resolution Spectroscopy I. Molecular Abundances

M. Lippi[1,2], G. L. Villanueva[1], M. J. Mumma[1], and S. Faggi[1,2]
[1] NASA Goddard Space Flight Center, Solar System Exploration Division, 8800 Greenbelt Road, Greenbelt, MD 20771, USA
[2] American University, Dept. of Physics, 4400 Massachusetts Avenue NW, Washington, DC 20016, USA
Received 2020 December 4; revised 2021 April 27; accepted 2021 April 27; published 2021 July 28

Abstract

We report and analyze updated molecular abundances in 20 comets obtained by employing modern data reduction procedures and molecular models. Using box and scatter plots, we examine how the different molecular species are distributed among the comet population, while by means of pie charts, we investigate the relative proportions of these molecular species in each comet. We compare these results with the orbital parameters of the selected comets to identify trends related to their dynamical history. With these analyses, we tentatively identify at least three chemical classes based mainly on relative abundances of CO, CH_3OH, CH_4, C_2H_6, HCN, and NH_3. The combination of relative abundances and orbital parameters is then compared with recent chemical models of planetary system formation. This approach may help in investigating the origins and evolution of the material in cometary nuclei. Among other aspects, we underline the need to increase our sample size, especially for hypervolatiles (i.e., CH_4 and CO) in Jupiter family comets.

Unified Astronomy Thesaurus concepts: Comets (280); Solar system formation (1530); Comet volatiles (2162)

Supporting material: tar.gz file

1. Introduction

Comets are cryogenically preserved relics from the formation of the solar system. They accumulated from the dusty and icy material present in the midplane of our protoplanetary disk system about 4.6 billion yr ago. After formation, they were scattered by strong gravitational interactions with the forming giant planets into their current dynamical reservoirs: the Oort Cloud (OC), considered the primary source of long-period and dynamically new comets, and the scattered disk of the Kuiper Belt (KB), the primary source of Jupiter family (JF) comets. According to current models (Levison & Morbidelli 2003; Gomes et al. 2005), most of the objects that formed between 5 and 17 au likely scattered into the OC reservoir, while those that formed in the outer protoplanetary disk (beyond $R_h \sim 17$ au) entered both the OC and KB reservoirs. Recent models also predict that a significant fraction of OC comets may have been captured from similar reservoirs surrounding other stars in the Sun's birth cluster (Levison et al. 2010). Once in their reservoirs, comet nuclei are likely to remain frozen, and the material below the surface layer will remain largely unaltered over time. Investigating their chemical composition and related properties may unveil the conditions present during their formation (e.g., radial temperature gradient, molecular abundances, and amount of UV/X-ray/cosmic-ray penetration into the protoplanetary disk) and reveal important clues to the early evolution of the solar system. Moreover, it could disclose which processes may have changed the nucleus composition after its formation (e.g., cosmic rays impacting the outer layer of the nucleus or successive surface warming on repeated passages through the inner solar system).

The organic composition of a comet nucleus can be studied in active comets using ground-based high-resolution spectroscopy that allows observations of emission lines produced by solar-pumped fluorescence of primary and product species, the first being those stored as native species within the nucleus, while the latter are produced in the coma by the dissociation of primary species. In the near-UV/visible spectral region (0.3–0.9 μm), product species such as OH, NH, CN, CH, C_2, C_3, and NH_2 have been observed in comets since 1860. Photometric observations in this spectral region revealed two distinct chemical classes, with about 30% of objects depleted in the C_2/CN ratio (A'Hearn et al. 1995). This trend is confirmed by optical spectral surveys at both high and low resolution (Fink 2009; Cochran et al. 2015). However, since diverse chemical and physical processes are involved in the production of secondary species and an individual secondary may have multiple possible precursors (Feldman et al. 2004), these abundances may not directly reflect the composition of the nucleus.

Primary volatiles such as H_2O, CO, H_2CO, CH_3OH, CH_4, C_2H_2, C_2H_6, HCN, and NH_3 have been studied in active comets using high-resolution spectroscopy in the infrared spectral region (2–5 μm) since 1985 (Mumma et al. 1986), revealing a significant chemical diversity among these bodies (see recent taxonomic reviews, e.g., Mumma & Charnley 2011; Dello Russo et al. 2016; Bockelée-Morvan & Biver 2017). Despite the increasing number of observed comets in the IR, taxonomic surveys based on primary species comprise smaller samples than those based on product species (usually about 30 targets or less), and there is yet no agreement on a prevalent classification.

In Lippi et al. (2020), we demonstrated that some previously reported infrared results may need revisiting due to the incomplete molecular models originally used to interpret the fluorescence emissions, insufficiently accurate atmospheric transmittances, and minor differences introduced by individual groups in the data analysis extraction methods. Our previous work showed that the employment of full quantum molecular models for the interpretation of cometary spectra (e.g., Villanueva et al. 2011b, 2012a, 2012b) combined with accurate terrestrial transmittance models retrieved at the time of observations (PUMAS/PSG; Villanueva et al. 2018) impact

mostly comets observed before 2011, when these novel analysis approaches started to be introduced. The reanalysis of their spectra is necessary to identify and remove potential biases before applying a reliable statistical analysis.

In this paper, we report updated molecular abundances (i.e., mixing ratios (MRs), % with respect to water) retrieved in 20 comets using the latest version of the data reduction procedures and models available in our team; the new results validate the need to verify and update results produced before 2011. We investigate the chemical diversity observed among the selected comets using a descriptive statistical approach to group similar objects and identify trends among the analyzed molecular species. We then compare our results with recent protoplanetary disk models and try to correlate our abundances with those that are expected in different regions of the disk midplane during the formation and evolution of the solar system. This paper is the first of a series aimed at exploring different cosmogonic indicators in comets (i.e., molecular abundances, ortho-to-para ratios, and isotopic ratios) obtained from a more consistent set of data based on infrared observations.

2. Data Reduction

The 20 comets[3] were selected from our archival database (see Lippi et al. 2020), considering observations performed with the NIRSPEC spectrometer situated at the W. M. Keck Observatory atop Maunakea in Hawaii (McLean et al. 1998). Except for comet C/1999 H1 (Lee), the spectra of all 20 comets are public domain data taken from the Keck-NIRSPEC archive, many of them observed by our group at the time, and now collected with many other spectra in our database. The targets, listed in Table 1 together with their observing logs and orbital parameters, were chosen after pondering the most sensitive data sets.

We reanalyzed each data set in a systematic way using semiautomated tools that improve processing speed and can help in reducing some forms of human error. Spectral calibration and compensation for telluric absorption was achieved by comparing the data with the atmospheric radiance and transmittance models synthesized with PUMAS/PSG (Villanueva et al. 2018). The PUMAS/PSG uses realistic profiles obtained from the most recent atmospheric database produced by NASA's Modern-Era Retrospective Analysis for Research and Applications (MERRA-2; Gelaro et al. 2017) together with the latest radiative transfer methods and spectroscopic parameters. In this way, we calculate line-by-line, layer-by-layer models for the terrestrial atmosphere under the specific observational conditions.

Flux calibration was obtained from the spectra of a standard star observed closely in time with the comet and now reduced with the same set of current algorithms. In fact, the flux conversion factors may also be impacted by the reanalysis, since they are retrieved by comparing the top-of-atmosphere stellar flux density ($W\,m^{-2}/cm^{-1}$) modified by the modeled atmospheric transmittance and the measured instrumental counts per pixel (ADU s^{-1}) at individual frequencies.

Rotational temperatures and production rates were obtained following the methodology introduced in our previous work (Lippi et al. 2020). First, for spectra with a sufficient signal-to-noise ratio and number of detected lines, we retrieved the rotational temperatures ($T_{\rm rot}$) using two different techniques: a χ^2 minimization Levenberg–Marquardt fitting algorithm (see Villanueva et al. 2008) and a correlation analysis (see Bonev 2005). Then, a fixed temperature value is chosen based on the most sensitive measurement for that night; usually, this value coincides with the rotational temperature for water. Once $T_{\rm rot}$ is determined, for each species, the line production rates ($Q_{\rm line}$) are calculated using the relationship

$$Q_{\rm line} = {\rm GF}\frac{4\pi\Delta^2 F_{\rm line}}{\tau_{\rm mol} f(x) g_{\rm line}},$$

where $F_{\rm line}$ is the line flux (Wm^{-2}, corrected for telluric transmittance at the Doppler-shifted line center), Δ is the geocentric distance (m), $\tau_{\rm mol}$ is the molecular photodissociation lifetime of the considered molecule (in seconds and calculated for a heliocentric distance of 1 au), $f(x)$ is a function representing the fraction of all targeted molecules in the coma contained in the beam (see the Appendix in Hoban et al. 1991), and GF is a growth factor accounting for slit losses and aperture effects (for details on the growth factor formalism, see, for example, Villanueva et al. 2011a, Appendix B2 in Dello Russo et al. 1998; Bonev et al. 2006). When analyzing growth factors, we symmetrized the spatial distribution measured about the nucleus at each distance from the nucleus-centered position and assumed a spherically symmetric uniform outflow $v_{\rm exp} = 0.8 r_h^{-0.5}$. The line g-factor ($g_{\rm line}$; W molecule^{-1}) is calculated at the determined rotational temperature (and for a heliocentric distance of 1 au). The final total production rate for each molecular species is computed as the weighted average of the production rates resulting from individual emission lines. The results from the line analysis are also compared with the ones obtained with the χ^2 minimization Levenberg–Marquardt fitting algorithm to check for consistency. For the analysis reported in this paper, in the case of nondetections, we make use of 2σ upper limits (corresponding to the 95% confidence limit) retrieved from the covariance matrix of the Levenberg–Marquardt fitting algorithm. We consider an upper limit significant only if it is smaller than the median value obtained from the corresponding box plot statistics (see Section 3.1).

Hereafter, we will always refer to MRs with respect to water. If a species is detected during multiple observing nights, the final MRs reported in Table 2 are calculated as the weighted mean of each single retrieved MR. The choice of using a weighted mean instead of a straight unweighted average comes from the assumption that MRs are intrinsic properties of a comet. In this respect, for the same comet, any variation that may be seen among different dates is probably more instrument- and noise-related rather than a real effect due to heterogeneity in composition; the weighted mean then ensures that the best data dominate. When we have both detections and 2σ upper limits, the latter are not included in this calculation; in fact, we observe that in some cases, upper limits versus detections are not consistent (see, for example, C_2H_2 in comet

[3] From now on, we will use the following acronyms and/or numbers to identify the analyzed comets: 1—C/2007 N3: C/2007 N3 (Lulin); 2—C/1999 S4: C/1999 S4 (LINEAR); 3—C/1999 H1: C/1999 H1 (Lee); 4—C/2009 P1: C/2009 P1 (Garradd); 5—C/2012 S1: C/2012 S1 (ISON); 6—C/2012 F6: C/2012 F6 (Lemmon); 7—C/1999 T1: C/1999 T1 (McNaught–Hartley); 8—C/2000 WM_1: C/2000 WM_1 (LINEAR); 9—C/2013 R1: C/2013 R1 (Lovejoy); 10—C/2001 A2: C/2001 A2 (LINEAR); 11—C/2004 Q2: C/2004 Q2 (Machholz); 12—C/2007 W1: C/2007 W1 (Boattini); 13—8P: 8P/Tuttle; 14—103P: 103P/Hartley 2; 15—73PB: 73P/Schwassmann–Wachmann (B); 16—73PC: 73P/Schwassmann–Wachmann (C); 17—17P: 17P/Holmes; 18—10P: 10P/Tempel 2; 19—9P: 9P/Tempel 1; 20—2P: 2P/Encke.

Table 1
Observing Logs and Orbital Parameters for the Analyzed Comets[a]

	Comet[b]	Log for the Observations				Orbital Parameters					
		Date Range	R_h (au)	Δ (au)	V_Δ (km s^{-1})	Dynamical Type[c]	T_J	q (au)	i (deg)	e	P (yr)
1	C/2007 N3 (Lulin)	31 Jan 2009	1.26	0.95	−54.2	OC–DN	−1.37	1.21	178.4	0.9999	1.95 10^7
		1 Feb 2009	1.26	0.92	−54.1						
2	C/1999 S4 (LINEAR)	13 Jul 2000	0.81	0.55	−54.6	OC–DN	−0.93	0.77	149.4	1.00	
3	C/1999 H1 (Lee)	19 Aug 1999	1.05	1.38	−28.3	OC	−0.90	0.71	149.4	0.9997	1.46 10^5
		20 Aug 1999	1.06	1.36	−29.0						
4	C/2009 P1 (Garradd)	13 Oct 2011	1.83	1.84	19.2	OC–DN	−0.43	1.55	106.2	1.001	
		9 Jan 2012	1.57	1.84	−20.9						
		10 Jan 2012	1.57	1.83	−21.2						
5	C/2012 S1 (ISON)	22 Oct 2013	1.21	1.50	−52.1	OC–DN	0.07	0.01	62.4	1.000	
		24 Oct 2013	1.17	1.44	−51.6						
		25 Oct 2013	1.15	1.41	−51.4						
		7 Nov 2013	0.83	1.06	−42.0						
6	C/2012 F6 (Lemmon)	20 Jun 2013	1.74	1.79	5.4	OC	0.15	0.73	82.6	0.9985	1.07 10^4
7	C/1999 T1 (McNaught–Hartley)	14 Jan 2001	1.28	1.35	−11.2	OC	0.23	1.17	80.0	0.9998	7.36 10^5
		5 Feb 2001	1.44	1.29	1.6						
		6 Feb 2001	1.45	1.29	2.3						
8	C/2000 WM_1 (LINEAR)	23 Nov 2001	1.35	0.38	−23.4	OC	0.28	0.56	72.6	1.000	
		24 Nov 2001	1.34	0.37	−21.3						
9	C/2013 R1 (Lovejoy)	22 Oct 2013	1.37	0.84	−40.0	OC	0.50	0.81	64.0	0.9984	1.17 10^4
		24 Oct 2013	1.34	0.79	−39.5						
		25 Oct 2013	1.33	0.77	−39.0						
		27 Oct 2013	1.30	0.73	−38.2						
		28 Oct 2013	1.29	0.70	−37.7						
		29 Oct 2013	1.28	0.68	−37.2						
10	C/2001 A2 (LINEAR)	9 Jul 2001	1.16	0.28	11.4	OC	0.88	0.78	36.5	0.9997	1.27 10^5
		10 Jul 2001	1.17	0.28	12.5						
11	C/2004 Q2 (Machholz)	28 Nov 2004	1.49	0.66	−21.8	OC	1.07	1.21	38.6	0.9995	1.18 10^5
		29 Nov 2004	1.48	0.64	−21.7						
		19 Jan 2005	1.21	0.39	11.2						
12	C/2007 W1 (Boattini)	9 Jul 2008	0.89	0.35	12.9	OC–DN	1.13	0.85	9.9	1.000	
		10 Jul 2008	0.90	0.36	13.0						
13	8P/Tuttle	22 Dec 2007	1.16	0.32	−19.2	HT	1.60	1.03	55.0	0.8198	13.6
		23 Dec 2007	1.15	0.31	−18.0						
14	103P/Hartley 2	16 Sep 2010	1.20	0.28	−12.0	JF	2.64	1.06	13.6	0.6949	6.5
		18 Sep 2010	1.19	0.26	−11.7						
		17 Oct 2010	1.07	0.13	−2.3						
		19 Oct 2010	1.07	0.12	−0.9						
		21 Oct 2010	1.06	0.12	0.6						
		22 Oct 2010	1.06	0.12	1.2						
		4 Nov 2010	1.06	0.16	7.0						
		16 Nov 2010	1.09	0.21	8.7						
15	73P/Schwassmann–Wachmann (B)	14 May 2006	1.00	0.07	0.3	JF	2.78	0.94	11.4	0.6933	5.4
		15 May 2006	1.00	0.07	2.0						
16	73P/Schwassmann–Wachmann (C)	14 May 2006	1.00	0.08	3.1	JF	2.78	0.94	11.4	0.6922	5.4
		15 May 2006	1.00	0.08	4.6						
17	17P/Holmes	27 Oct 2007	2.45	1.63	−3.3	JF	2.86	2.06	19.1	0.4318	6.9
		30 Oct 2007	2.46	1.62	−2.3						
18	10P/Tempel 2	26 Jul 2010	1.44	0.69	−4.2	JF	2.96	1.42	12.0	0.5363	5.4
19	9P/Tempel 1	3 Jun 2005	1.54	0.76	5.5	JF	2.97	1.54	10.5	0.5096	5.6
		4 Jul 2005	1.51	0.89	9.2						
		5 Jul 2005	1.51	0.89	9.3						
20	2P/Encke	4 Nov 2003	1.21	0.31	−13.4	JF–ET	3.03	0.34	11.8	0.8483	3.3
		5 Nov 2003	1.19	0.31	−12.5						
		6 Nov 2003	1.18	0.30	−11.5						

Notes.
[a] Ephemeris and orbital parameters are from the HORIZONS Web Interface and the JPL Small-Body Database Browser, respectively.
[b] Comets are ordered with increasing Tisserand parameter.
[c] JF = Jupiter family, ET = Encke type, HT = Halley type, OC = Oort Cloud, DN = dynamically new.

Table 2
Updated MRs (% Relative to Water) Measured for the Selected Comets

	Comet[i]	CH_3OH	HCN	NH_3	H_2CO	C_2H_2	C_2H_6	CH_4	CO
1	**C/2007 N3**	3.82 ± 0.15	0.14 ± 0.01	0.27 ± 0.16	0.15 ± 0.02	0.08 ± 0.02	0.80 ± 0.04	1.30 ± 0.07	2.66 ± 0.15
2	**C/1999 S4**	<0.13	0.04 ± 0.02	<0.76[viii]	<0.06	<0.05	0.11 ± 0.02	0.22 ± 0.06	1.36 ± 0.32
3	**C/1999 H1**	3.20 ± 0.16	0.19 ± 0.02	0.56 ± 0.15	0.24 ± 0.04	0.09 ± 0.02	0.89 ± 0.04	1.07 ± 0.09	1.48 ± 0.37
4	**C/2009 P1**	2.29 ± 0.18	0.24 ± 0.02	1.03 ± 0.81	<0.05	0.16 ± 0.04	0.67 ± 0.05	1.02 ± 0.07	7.71 ± 2.13
5	**C/2012 S1**	<1.2	0.10 ± 0.02	<0.68	<0.09[vii]	0.11 ± 0.05	0.41 ± 0.09	0.41 ± 0.06	<2.52
6	**C/2012 F6**[ii]	1.46 ± 0.20	0.19 ± 0.04	0.58 ± 0.23	<0.05	<0.05	0.31 ± 0.04	0.67 ± 0.11	4.03 ± 0.45
7	**C/1999 T1**	3.65 ± 0.38	0.15 ± 0.03	<1.1[vii]	0.14 ± 0.05	0.28 ± 0.07	1.04 ± 0.13	2.72 ± 1.63	13. ± 2.6
8	**C/2000 WM_1**	1.23 ± 0.08	0.21 ± 0.01	<0.42	0.06 ± 0.02	0.06 ± 0.02	0.51 ± 0.02	0.41 ± 0 .03	0.69 ± 0.22
9	**C/2013 R1**	2.92 ± 0.20	0.24 ± 0.01	1.48 ± 0.28	0.08 ± 0.03	0.08 ± 0.01	0.65 ± 0.04	1.17 ± 0.04	7.97 ± 0.51
10	**C/2001 A2**	4.11 ± 0.25	0.30 ± 0.02	<0.51	0.08 ± 0.02	0.14 ± 0.02	2.73 ± 0.15	1.79 ± 0.17	3.07 ± 0.96
11	**C/2004 Q2**	1.82 ± 0.06	0.157 ± 0.009	0.24 ± 0.01	0.062 ± 0.008	0.068 ± 0.009	0.69 ± 0.03	1.32 ± 0.06	4.83 ± 0.66
12	**C/2007 W1**	4.13 ± 0.29	0.22 ± 0.02	0.76 ± 0.14	<0.02	0.13 ± 0.02	0.92 ± 0.06	0.78 ± 0.15	1.83 ± 0.31
13	**8P**	2.61 ± 0.13	0.16 ± 0.02	0.72 ± 0.38	0.10 ± 0.02	<0.04	0.30 ± 0.03	0.25 ± 0.02	<0.84
14	**103P**[iii]	2.32 ± 0.05	0.259 ± 0.007	0.64 ± 0.06	0.08 ± 0.02	0.105 ± 0.008	0.87 ± 0.01	<0.8[viii]	0.30 ± 0.15
15	**73PB**[iv]	0.41 ± 0.05	0.259 ± 0.008	<0.20	0.03 ± 0.01	0.03 ± 0.01	0.204 ± 0.008	<0.17	0.53 ± 0.13
16	**73PC**[iv]	0.47 ± 0.05	0.299 ± 0.007	<0.15	0.051 ± 0.006	0.029 ± 0.009	0.136 ± 0.004	<0.17	0.53 ± 0.13
17	**17P**[v]	4.30 ± 0.43	0.61 ± 0.09	0.82 ± 0.52	<0.16[vii]	0.24 ± 0.11	2.31 ± 0.14	N.A.	8.8 ± 2.7
18	**10P**[vi]	1.81 ± 0.21	0.12 ± 0.02	1.12 ± 0.24	<0.09[viii]	<0.06	0.43 ± 0.04	N.A.	N.A.
19	**9P**	2.22 ± 0.19	0.24 ± 0.03	1.14 ± 0.72	0.18 ± 0.07	<0.07	0.36 ± 0.04	0.66 ± 0.30	<2.65
20	**2P**	3.56 ± 0.27	0.08 ± 0.01	<0.47	<0.07	<0.05	0.54 ± 0.05	0.48 ± 0.06	<1.9
	Median	**2.61**	**0.21**	**0.75**	**0.08**	**0.10**	**0.65**	**0.78**	**2.66**

Notes.
[i] Comets are ordered following increasing Tisserand parameter.
[ii] The CH_4 is from Paganini et al. (2014).
[iii] The CO is from Weaver et al. (2011).
[iv] The CO is from DiSanti et al. (2007), while CH_4 is from Villanueva et al. (2006); we used common values for both fragments.
[v] It was not possible to measure CH_4 in 17P.
[vi] It was not possible to measure CO and CH_4 in 10P.
[vii] The upper limit is much greater than the median, and we consider it not significant.
[viii] The upper limit is comparable to the median, and we consider it significant.

C/2009 P1 or H_2CO in comet C/2000 WM_1). We believe that these upper limits, strongly dependent on the stochastic noise, would bias our results if included. If for a molecular species we don't have any detection, we assume as representative the lowest of the measured upper limits.

In Appendix A, we compiled for each comet[4] a dedicated section that comprises a short description of the observing time and conditions, the comparisons with previously reported results, and a short discussion of the factors that may have contributed to the observed differences with respect to past results. Associated summary tables with our results (rotational temperatures, nucleus-centered production rates, growth factors, global production rates, and date-by-date MRs that we used to calculate the final values reported in Table 2) are provided online, in machine-readable format (see link in Appendix A).

In Table 3, we compare our MRs with those retrieved in the past; relevant references to previous works are indicated in the table notes. It is possible to see that the largest dissimilarities occur among targets analyzed before 2011. Since these differences depend on a mix of corrections introduced by the new analysis, it is not easy to identify if a specific factor's influence is stronger than the others. One notable change in the current algorithms is the inclusion of full cascade contributions to a given emission line. The effect is to increase the modeled *g*-factor and thus lower the derived column density needed to produce the observed line flux. Using the model for water presented in Villanueva et al. (2012b), we usually retrieve similar-to-lower production rates for this molecule with respect to the previously reported ones (see comet-by-comet comparisons in Appendix A). If we combine this with the use of complete quantum molecular models for the other species (for example, CH_3OH: Villanueva et al. 2012a; C_2H_6: Villanueva et al. 2011b; HCN and NH_3: Villanueva et al. 2013), the differences in retrieved MRs can be considerable. For example, for CH_3OH, we observe an average increment of about 70% in comets studied before 2011, while for comets analyzed after 2011, this increment is only about 7% (i.e., values are usually comparable within 1σ uncertainties). The large differences we observe are indeed related to the use of more suitable models in place of empirical *g*-factors employed in the past that allowed the analysis of a few emission lines only (e.g., the *Q* branch of the CH_3OH–ν_3 transition). The use of full quantum molecular models also allows the identification of several blended lines not recognized before, especially in crowded spectral regions. This further impacts the retrieved production rates and MRs of C_2H_6, CH_3OH, and CH_4 in the CH-stretching region and HCN, C_2H_2, and NH_3 in the CN-stretching region (see the example of HCN and water in comet C/1999 S4 in Lippi et al. 2020). Finally, it is possible to notice that for many spectra analyzed before 2011, some species were not investigated because proper molecular fluorescence models were lacking (e.g., NH_3 and H_2CO). With our reanalysis, we managed to add these missing values, or at least retrieve corresponding 2σ upper limits, producing a more inclusive statistical sample.

[4] Except for the comets already described in Lippi et al. (2020).

Table 3
Comparison with Previously Reported MRs Relative to Water[i]

	Comet		CH_3OH	HCN	NH_3	H_2CO	C_2H_2	C_2H_6	CH_4	CO
1	**C/2007 N3**	TW	3.82 ± 0.15	0.14 ± 0.01	0.27 ± 0.16	0.15 ± 0.02	0.08 ± 0.02	0.80 ± 0.04	1.30 ± 0.07	2.66 ± 0.15
		PW[ii] (2012)	3.62 ± 0.18	0.124 ± 0.009	0.28 ± 0.06	0.11 ± 0.02	0.066 ± 0.011	0.86 ± 0.04	1.19 ± 0.06	2.17 ± 0.11
		D%	+5.5%	+12.9%	−3.6%	+36.4%	+21.2%	−7.0%	+9.2%	+22.6%
2	**C/1999 S4**					See Lippi et al. 2020				
3	**C/1999 H1**	TW	3.20 ± 0.16	0.19 ± 0.02	0.56 ± 0.15	0.24 ± 0.04	0.09 ± 0.02	0.89 ± 0.04	1.07 ± 0.09	1.48 ± 0.37
		PW[iii] (2001)	2.1 ± 0.5	0.23 ± 0.02	⋯	⋯	0.27 ± 0.03	0.67 ± 0.07	0.81 ± 0.08	1.8 ± 0.8
		PW[iv] (2006)	1.6 ± 0.2	0.20 ± 0.02	⋯	⋯	0.24 ± 0.03	0.71 ± 0.07	1.13 ± 0.25	⋯
		D%	+52.4%	−17.4	⋯	⋯	−66.7%	+32.8%	+32.1%	−17.8%
			+100.0%	−5.0%			−62.5%	+25.4%	−5.3%	⋯
4	**C/2009 P1**	TW	2.29 ± 0.18	0.24 ± 0.02	1.03 ± 0.81	<0.05	0.16 ± 0.04	0.67 ± 0.05	1.02 ± 0.07	7.71 ± 2.13
		PW[v] (2014)	2.14 ± 0.38	0.22 ± 0.01	0.50 ± 0.16	0.11 ± 0.04	0.06 ± 0.02	0.64 ± 0.10	0.84 ± 0.08	9.12 ± 0.80
		D%	+7.0%	+9.1%	+106.0%	⋯	+166.7%	+4.7%	+21.4%	−15.5%
5	**C/2012 S1**					See Lippi et al. 2020				
6	**C/2012 F6**					See Lippi et al. 2020				
7	**C/1999 T1**	TW	3.65 ± 0.38	0.15 ± 0.03	<1.1	0.14 ± 0.05	0.28 ± 0.07	1.04 ± 0.13	2.72 ± 1.63	13.5 ± 2.6
		PW[vi] (2001–2003)	1.7 ± 0.5	0.37 ± 0.08	⋯	⋯	⋯	0.65 ± 0.13	1.4 ± 0.8	17 ± 5
		D%	+114.7%	−59.5%	⋯	⋯	⋯	+60.0%	+94.3%	−20.6%
8	**C/2000 WM_1**	TW	1.23 ± 0.08	0.21 ± 0.01	<0.42	0.06 ± 0.02	0.06 ± 0.02	0.51 ± 0.02	0.41 ± 0 .03	0.69 ± 0.22
		PW[vii] (2010)	1.30 ± 0.08	0.15 ± 0.01	⋯	0.20 ± 0.03	<0.03	0.47 ± 0.03	0.34 ± 0.03	0.52 ± 0.12
		D%	−5.4%	+40.0%	⋯	−70.0%	⋯	+8.5%	+20.6%	+32.7%
9	**C/2013 R1**	TW	2.92 ± 0.20	0.24 ± 0.01	1.48 ± 0.28	0.11 ± 0.03	0.09 ± 0.01	0.65 ± 0.04	1.17 ± 0.04	7.97 ± 0.51
		PW[viii] (2014)	2.75 ± 0.38	0.26 ± 0.02	0.10 ± 0.02	<0.04	<0.05	0.69 ± 0.06	0.89 ± 0.06	9.89 ± 2.03
		D%	+6.2%	−7.7%	+1380%	⋯	⋯	−5.8%	+31.5%	−19.4%
10	**C/2001 A2**					See Lippi et al. 2020				
11	**C/2004 Q2**	TW	1.82 ± 0.06	0.157 ± 0.009	0.24 ± 0.01	0.062 ± 0.008	0.068 ± 0.009	0.69 ± 0.03	1.32 ± 0.06	4.83 ± 0.66
		PW[ix] (2009)	2.14 ± 0.08	0.156 ± 0.009	0.37 ± 0.06	0.11 ± 0.02	0.09 ± 0.01	0.56 ± 0.02	1.47 ± 0.05	5.07 ± 0.51
		D%	−15.0%	+0.6%	−35.1%	−43.6%	−24.4	+23.2%	−10.2%	−4.7%
12	**C/2007 W1**					See Lippi et al. 2020				
13	**8P**	TW	2.61 ± 0.13	0.16 ± 0.02	0.72 ± 0.38	0.10 ± 0.02	<0.04	0.30 ± 0.03	0.25 ± 0.02	<0.84
		PW[x] (2008)	2.18 ± 0.07	0.07 ± 0.01	⋯	<0.03	<0.03	0.24 ± 0.03	0.37 ± 0.07	<0.25
		D%	+19.7	+128.6%	⋯	⋯	⋯	25.0%	−32.4%	⋯
14	**103P**	TW	2.32 ± 0.05	0.259 ± 0.007	0.64 ± 0.06	0.08 ± 0.02	0.105 ± 0.008	0.87 ± 0.01	<0.8	⋯
		PW[xi] (2011–2013)	1.60 ± 0.04	0.235 ± 0.005	0.87 ± 0.02	0.12 ± 0.02	0.106 ± 0.005	0.76 ± 0.02	<0.3	⋯
		D%	+45.0%	+10.2%	−26.4%	−33.3%	−0.94%	+14.5%	⋯	⋯
15	**73PB**	TW	0.41 ± 0.05	0.259 ± 0.008	<0.20	0.03 ± 0.01	0.03 ± 0.01	0.204 ± 0.008	⋯	⋯
		PW[xii] (2007)	0.20 ± 0.02	0.28 ± 0.01	<0.11	0.14 ± 0.02	0.026 ± 0.011	0.18 ± 0.01	⋯	⋯
		D%	+105%	−7.5%	⋯	−78.6%	+15.4%	+13.3%		
16	**73PC**	TW	0.47 ± 0.05	0.299 ± 0.007	<0.15	0.051 ± 0.006	0.029 ± 0.009	0.136 ± 0.004	⋯	⋯
		PW[xii] (2007)	0.19 ± 0.02	0.221 ± 0.008	<0.19	0.11 ± 0.02	0.05 ± 0.02	0.113 ± 0.007	⋯	⋯

Table 3
(Continued)

Comet			CH_3OH	HCN	NH_3	H_2CO	C_2H_2	C_2H_6	CH_4	CO
		D%	+147.4%	+35.3%	⋯	−53.6%	−42.0%	+20.4%	⋯	⋯
17	**17P**	TW	4.30 ± 0.43	0.61 ± 0.09	0.82 ± 0.52	<0.16	0.24 ± 0.11	2.31 ± 0.14	⋯	⋯
		PW[xiii] (2008)	2.37 ± 0.40	0.54 ± 0.08	⋯	⋯	0.34 ± 0.05	1.80 ± 0.23	⋯	⋯
		D%	+81.4%	+13.0%	⋯	⋯	−29.4%	+28.3%		
18	**10P**	TW	1.81 ± 0.21	0.12 ± 0.02	1.12 ± 0.24	<0.09	<0.06	0.43 ± 0.04	⋯	⋯
		PW[xiv] (2012)	1.58 ± 0.23	0.13 ± 0.02	0.83 ± 0.20	<0.07	<0.05	0.39 ± 0.04	⋯	⋯
		D%	+14.6%	−7.7 %	+34.9%	⋯	⋯	+10.3%		
19	**9P**	TW	2.22 ± 0.19	0.24 ± 0.03	1.14 ± 0.72	0.18 ± 0.07	<0.07	0.36 ± 0.04	0.66 ± 0.30	<2.65
		PW[xv](2005)	1.12 ± 0.12	0.20 ± 0.03	⋯	0.84 ± 0.18	0.13 ± 0.04	0.29 ± 0.02	0.54 ± 0.30	4.3 ± 1.2
		D%	+98.2%	+20.0%	⋯	−78.6%	⋯	+24.1%	+22.2%	⋯
20	**2P**	TW	3.56 ± 0.27	0.08 ± 0.01	<0.47	<0.07	<0.05	0.54 ± 0.05	0.48 ± 0.06	<1.9
		PW[xvi] (2013)	3.48 ± 0.27	0.09 ± 0.01	⋯	<0.09	<0.05	0.31 ± 0.03	0.34 ± 0.10	<1.2
		D%	+2.3%	−11.1 %	⋯	⋯	⋯	+74.2 %	+41.2%	⋯

Notes.
[i] Here TW stands for this work, PW stands for previous work, and D% stands for fractional difference in percent. To facilitate the comparisons, previously reported 3σ upper limits are converted to 2σ upper limits; comets are ordered as in Tables 1 and 2. Superscripts refer to source papers.
[ii] Gibb et al. (2012).
[iii] Mumma et al. (2001b).
[iv] Dello Russo et al. (2006).
[v] DiSanti et al. (2014).
[vi] Mumma et al. (2001a, 2003); Gibb et al. (2003).
[vii] Radeva et al. (2010).
[viii] Paganini et al. (2014).
[ix] Bonev et al. (2009).
[x] Bonev et al. (2008).
[xi] Weighted average of data from Dello Russo et al. (2011), Mumma et al. (2011), and Kawakita et al. (2013).
[xii] Dello Russo et al. (2007).
[xiii] Dello Russo et al. (2008).
[xiv] Paganini et al. (2012).
[xv] Mumma et al. (2005).
[xvi] Radeva et al. (2013).

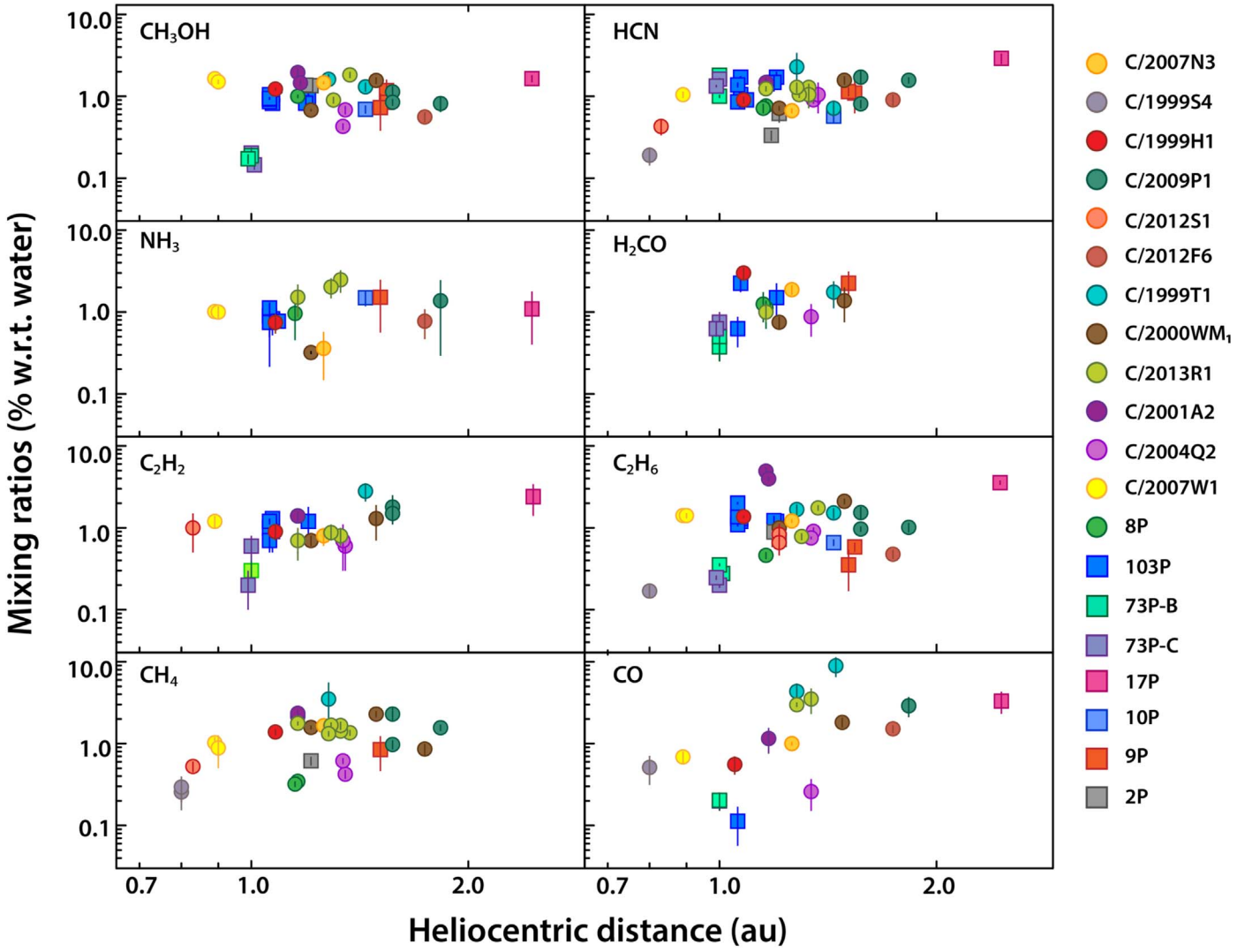

Figure 1. Measured MRs (relative to H_2O and normalized to the median) as a function of the heliocentric distance at the time of observations for the studied comets. Each color represents a different comet, as indicated in the legend on the right side. Upper limits are not reported.

There is evidence in some comets of possible outgassing variability at different heliocentric distances that can influence to some extent the resulting MRs relative to water (see, for example, Mumma et al. 2011; Faggi et al. 2019; Mumma et al. 2019). Also, comets observed farther than 1.5 au from the Sun may have a small tendency to show higher abundances of hypervolatiles with respect to other molecules (see, for example, Gicquel et al. 2015); comets with a perihelion distance beyond 2 au show strong effects of this kind (e.g., C/2006 W3; Bonev et al. 2017). The relationships between our measured MRs (normalized to their median) and the heliocentric distances at the time of observations are shown in Figure 1. In general, we do not see these effects, even if a certain trend seems to exist for CO. Most of our targets were observed between about 0.8 and 1.5 au, where water is fully active,[5] and we do not expect a strong influence of the heliocentric distance on our results. Considering our small sample and the limited orbital range for each analyzed comet, we are not able to determine if an evolution of the outgassing occurred along the orbit or the measured values are completely independent from the heliocentric distances. In the following analyses, we will assume the retrieved values to be representative of the nuclear original abundances. Yet we emphasize the need for detailed observing campaigns for each comet that test if and how the MRs vary with the heliocentric distance and to consider additional statistics derived from alternative abundance ratios (e.g., MRs calculated with respect to ethane; Mumma et al. 2017, 2018, 2019; Bonev et al. 2020). These investigations will be presented elsewhere.

[5] The exceptions are comets C/2012 F6, observed at 1.74 au, and 17P, observed at about 2.5 au (outburst).

3. Data Analysis and Discussion

3.1. Box Plot Statistics

We investigated the distribution of molecular species among the comet population making use of box plots, as shown in Figure 2 (absolute values in panel (a), values normalized to the median in panel (b)). The box plot statistics are calculated using the MRs reported in Table 2, which are graphed as filled circles on the right side of each box. We did not include in the calculation the 2σ upper limits. In fact, even if this reduces the already small size of our statistical sample, 2σ upper limit measurements are not always consistent with detections,

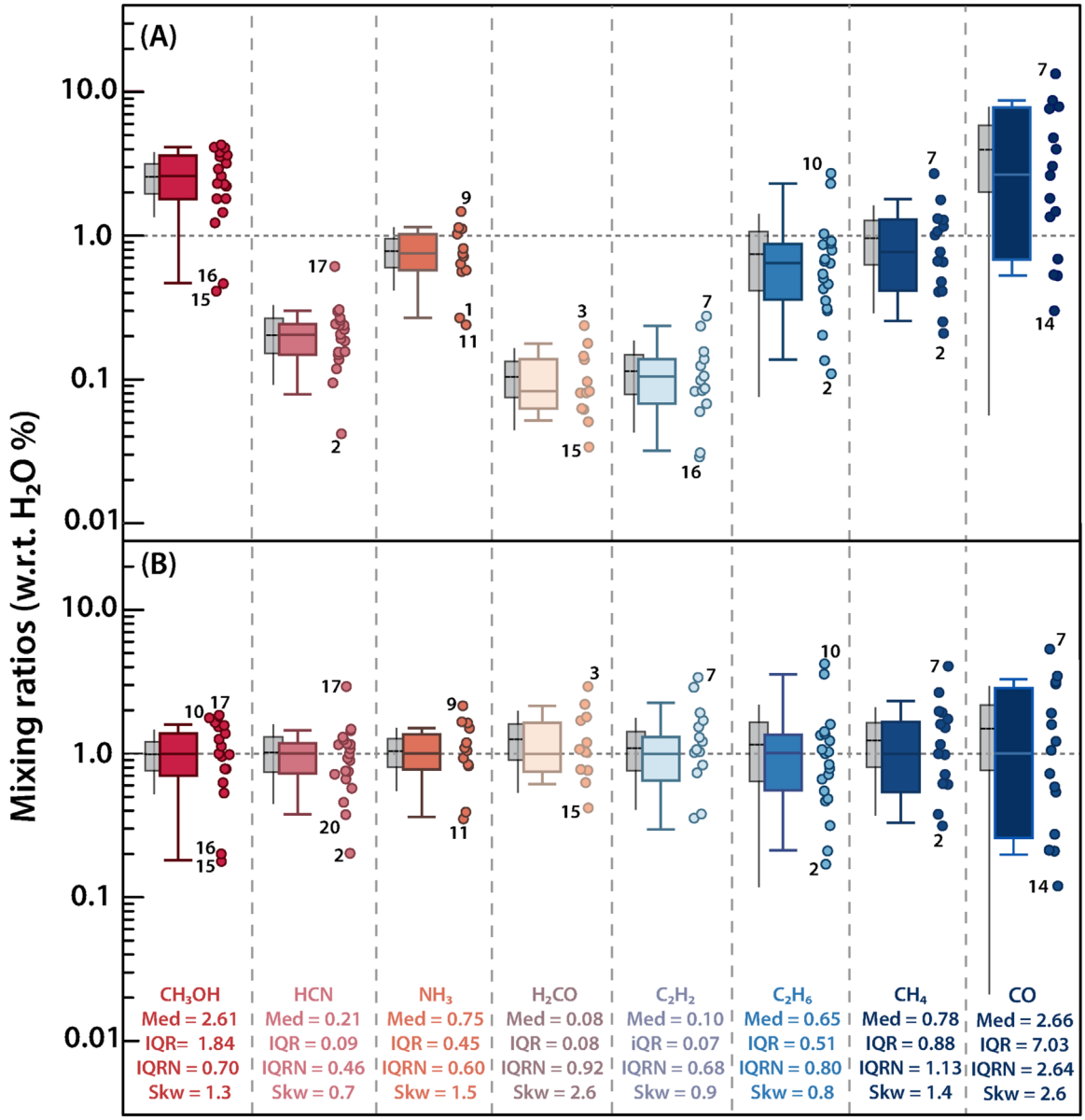

Figure 2. Box plot statistics obtained using absolute values of MRs (panel (a)) and MRs normalized to the median (panel (b)). The boxes are ordered and colored by sublimation temperature, with dark red corresponding to the highest temperature and dark blue to the lowest one. For each distribution, we report at the bottom of the plot the median (Med), interquartile range (IQR), IQRN, and skewness (Skw). The median is also shown with a horizontal line across each box. Outlier values with respect to the whiskers are highlighted with the corresponding comet's individual number (see Table 1). Each box is compared with a Gaussian distribution, represented as a symmetric gray box centered on the mean and described by the standard deviation of the data (1σ for the box limits, 2σ for the whiskers). The complete statistic for each box is reported in Table 4.

especially for NH_3, C_2H_2, and H_2CO, and we prefer to prevent the influence of these numbers on the statistics. The upper and lower bounds of each box are fixed at the 75th and 25th percentiles of the distribution, respectively. The whiskers are estimated using the 9th and 91st percentiles. The boxes are shown with a logarithmic scale and are compared with a Gaussian (symmetric box) centered on the mean and described by the standard deviation of the data (1σ for the box limits, 2σ for the whiskers). The box plot statistics are reported in Table 4. The molecules CO and CH_3OH show the highest median values (2.66 and 2.61, respectively), followed by CH_4 (0.78), NH_3 (0.75), and C_2H_6 (0.65). If we consider the interquartile range normalized to the median (IQRN), calculated as the difference between the 75th and the 25th percentile bounds, CO presents the highest dispersion (2.64), followed by CH_4 (1.13), H_2CO (0.92), C_2H_6 (0.80), CH_3OH (0.70), C_2H_2 (0.68), NH_3 (0.60), and HCN (0.46).

We calculated the skewness (Skw) of each box distribution as

$$\mathrm{Skw} = \frac{(75\text{th percentile} - 50\text{th percentile})}{(50\text{th percentile} - 25\text{th percentile})}.$$

Almost all analyzed molecular species are described by an upper-skewed (right-skewed; $\mathrm{Skw} > 1$) distribution, with the exceptions of C_2H_6 and HCN, which are instead lower-skewed (left-skewed; $\mathrm{Skw} < 1$); C_2H_2 is quasi-symmetric with respect to the median. If we assume that the studied molecular species should be normally distributed among comets, the separation from the Gaussian shape that we observe in our box plots could

Table 4
Box Plot Statistics

	CH_3OH	HCN	NH_3	H_2CO	C_2H_2	C_2H_6	CH_4	CO
Number of used points	18	20	12	12	14	20	15	15
9th percentile	0.47	0.08	0.27	0.05	0.03	0.14	0.25	0.53
(normalized value)[a]	(0.18)	(0.38)	(0.36)	(0.61)	(0.31)	(0.21)	(0.33)	(0.20)
25th percentile	1.82	0.15	0.58	0.06	0.07	0.36	0.41	0.69
(normalized value)[a]	(0.70)	(0.72)	(0.77)	(0.75)	(0.65)	(0.55)	(0.53)	(0.26)
Median—50th percentile	2.61	0.21	0.75	0.08	0.10	0.65	0.78	2.66
75th percentile	3.65	0.24	1.03	0.14	0.14	0.87	1.29	7.71
(normalized value)[a]	(1.40)	(1.18)	(1.36)	(1.66)	(1.32)	(1.35)	(1.67)	(2.90)
91st percentile	4.13	0.30	1.14	0.18	0.24	2.31	1.79	8.79
(normalized value)[a]	(1.58)	(1.46)	(1.51)	(2.16)	(2.25)	(3.58)	(2.30)	(3.30)
Interquartile range	1.84	0.09	0.45	0.08	0.07	0.51	0.88	7.03
Normalized IQRN[a]	0.70	0.46	0.60	0.92	0.68	0.80	1.13	2.64
Skewness[b]	1.31	0.67	1.54	2.62	0.92	0.77	1.43	2.56
Average	2.57	0.21	0.78	0.10	0.11	0.74	0.95	3.95
Standard deviation	1.23	0.12	0.36	0.06	0.07	0.67	0.67	3.89
Min. value	0.41	0.04	0.24	0.03	0.03	0.11	0.21	0.30
Max. value	4.30	0.61	1.48	0.24	0.28	2.73	2.73	13.5

Notes.
[a] Normalized with respect to the median.
[b] Calculated as (75th percentile – 50th percentile)/(50th percentile – 25th percentile).

be a bias related to the small size of our sample. However, an asymmetric box plot could also be indicative of a bimodal or multimodal distribution, compatible with distinct chemical populations of comets. Additional data are needed to improve these statistics.

Our median and average values agree within the error bars with the average MRs (% relative to water) calculated for a sample of 30 comets in Dello Russo et al. (2016), except for H_2CO, for which we find a much lower value. Despite the similarities, our averages are characterized by higher standard deviations, especially for hypervolatile species, most likely related to the smaller size of our sample.

We examined the relationships between our MRs and the corresponding Tisserand invariant (T_J, with respect to Jupiter), as shown in Figure 3. While it is not possible to identify very strong relationships between MRs and T_J in comets, data for C_2H_6, CH_4, and CO display more pronounced dispersions, with OC comets showing higher values than JF comets, even if exceptions are present (see, for example, CO in comet C/2000 WM_1 or C_2H_6 and CH_4 in comet C/1999 S4). It is important to note that many reported MR values for CH_4 and CO in JF comets consist of 2σ upper limits, so that many more measurements of these two species in JF comets are necessary to recognize clearer trends.

3.2. Relative Abundances of the Volatile Species in Comets: Pie Charts

We compared 18 comets[6] using double-level pie charts (see Figures 4 and 5). The inner level of each pie considers chemical functional groups in the following way: (1) CO and H_2CO (carbonyl and aldehyde groups) in red; (2) CH_3OH (alcohol group) in yellow; (3) C_2H_6, CH_4, and C_2H_2 (hydrocarbon group) in green; and (4) HCN (nitrile group) in blue. In the outer level, we instead describe each molecular species separately. In the first analysis, we have not included the NH_3 contribution, which we show instead in Figure 6.[7] We decided to show these as separate pies because in our spectra, ammonia abundances are usually retrieved using only one or two faint spectral lines and are often characterized by large uncertainties. This also happens with other molecules, notably H_2CO and C_2H_2, but while MRs for the latter are usually described by quite low values, NH_3 may assume values comparable to those retrieved for molecules such as CH_3OH and CO and can significantly influence the shape of the pies (see, for example, comet C/1999 S4).

From the first and second group of pie charts (Figures 4 and 5), we notice that even though the analyzed comets show a variety of different compositions, they could possibly be divided into two main groups. Comets C/1999 S4, C/2009 P1, C/1999 T1, C/2013 R1, C/2012 F6, C/2004 Q2, and C/2012 S1 show a high amount of carbonyl material with respect to other functional groups. Except for C/1999 S4, the MRs of methanol in these comets are comparable to those of the hydrocarbon group. Methane is the dominant species among the hydrocarbons, with MRs that are typically twice those of C_2H_6 (except for comet C/2012 S1). Comets in the second group of pies, however, show a lower amount of CO and can be divided into two subgroups; while C/2007 N3, C/1999 H1, and 9P still show a higher amount of CH_4 with respect to ethane, most other comets show CH_4 MRs that are comparable to or lower than C_2H_6 MRs.

It is possible that comets of the first group formed in a warmer region of the midplane, where CH_3OH and hydrocarbons were not efficiently produced (Geppert et al. 2006 Garrod et al. 2006), and CO and CH_4 were trapped in dust grains and sufficiently shielded from the radiation field by the dust (Kama et al. 2016), so that these comets may have incorporated less chemically processed material. On the other hand, comets belonging to the second group show proportions of material that could be indicative of efficient hydrogenation processes, suggesting that these comets formed in colder

[6] We excluded 17P and 10P, since we do not have any measurements for CO and CH_4 in them.

[7] We excluded comet C/1999 T1 because the 2σ upper limit for NH_3 is not significant with respect to our statistic.

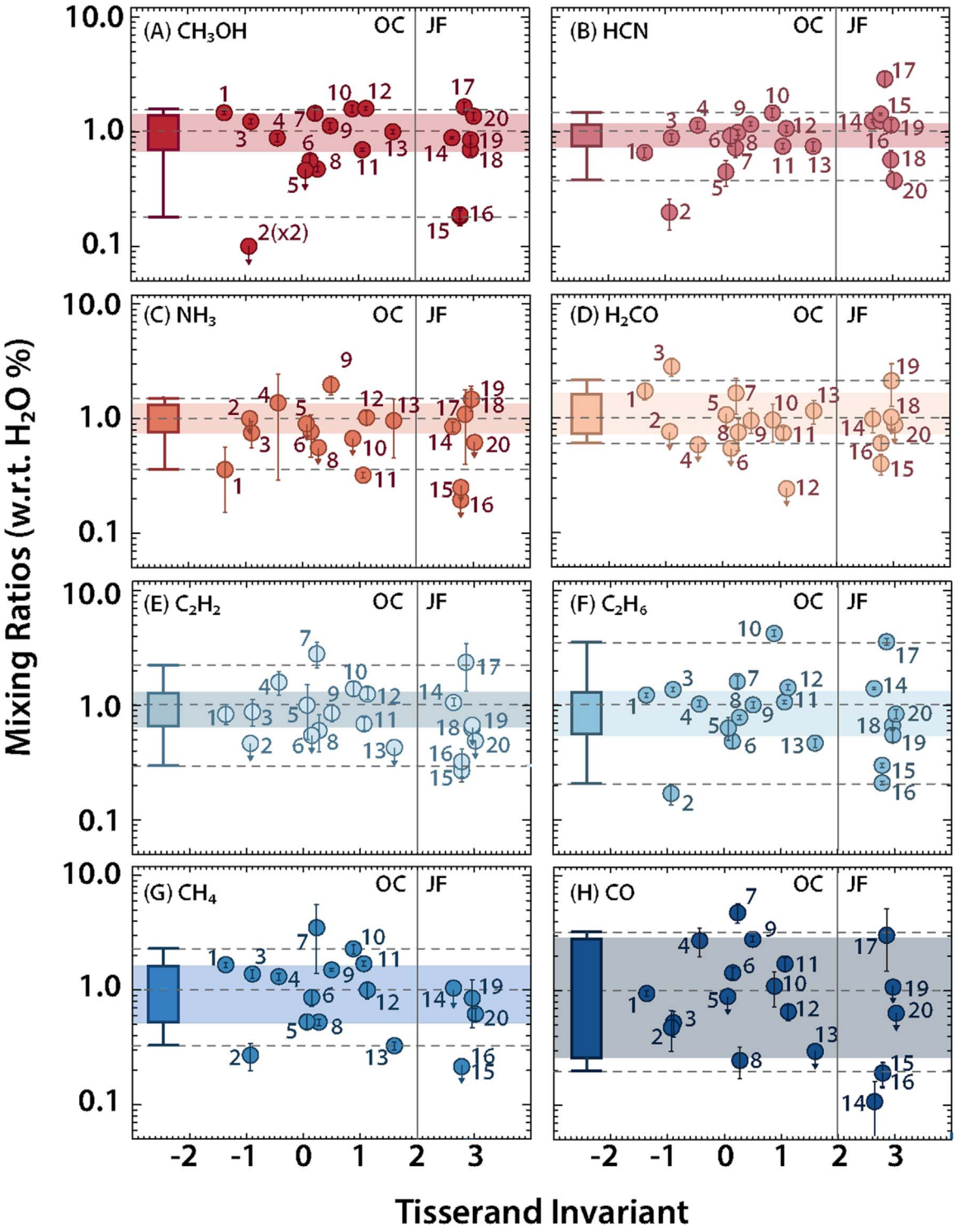

Figure 3. Measured MRs normalized to the median as a function of the Tisserand invariant. For each plot, the data are reported with their corresponding error bars, while downward arrows represent 2σ upper limits (2σ upper limits that are not significant are not shown). For each molecule, the ranges of 25th–75th percentiles are shown as colored horizontal bars, following the same color codes as in Figure 2, while medians and 9th and 91st percentiles are shown as horizontal dashed lines. A vertical solid line separates OC and JF comets. The data are numbered according to increasing Tisserand invariant (see Table 1).

environments. The higher amount of ethane with respect to methane in some comets may be related to significant processing of the material by the UV/X-ray/cosmic-ray radiation field and later conversion to ethane via successive hydrogenations (Bosman et al. 2018 and references therein).

When including the contribution of ammonia, we see basically the same grouping of comets; C/2013 R1, C/2009 P1, C/2012 F6, C/2012 S1, C/2004 Q2, and C/1999 S4 still show CO as the dominant molecular species. But while the first four comets show similar amounts of NH_3 and the sum of nitriles comparable to the sum of hydrocarbons, C/2004 Q2 looks much depleted in ammonia; the high value shown in C/1999 S4 instead is a 2σ upper limit, and the actual abundance could indeed be compatible with this group. For all of these

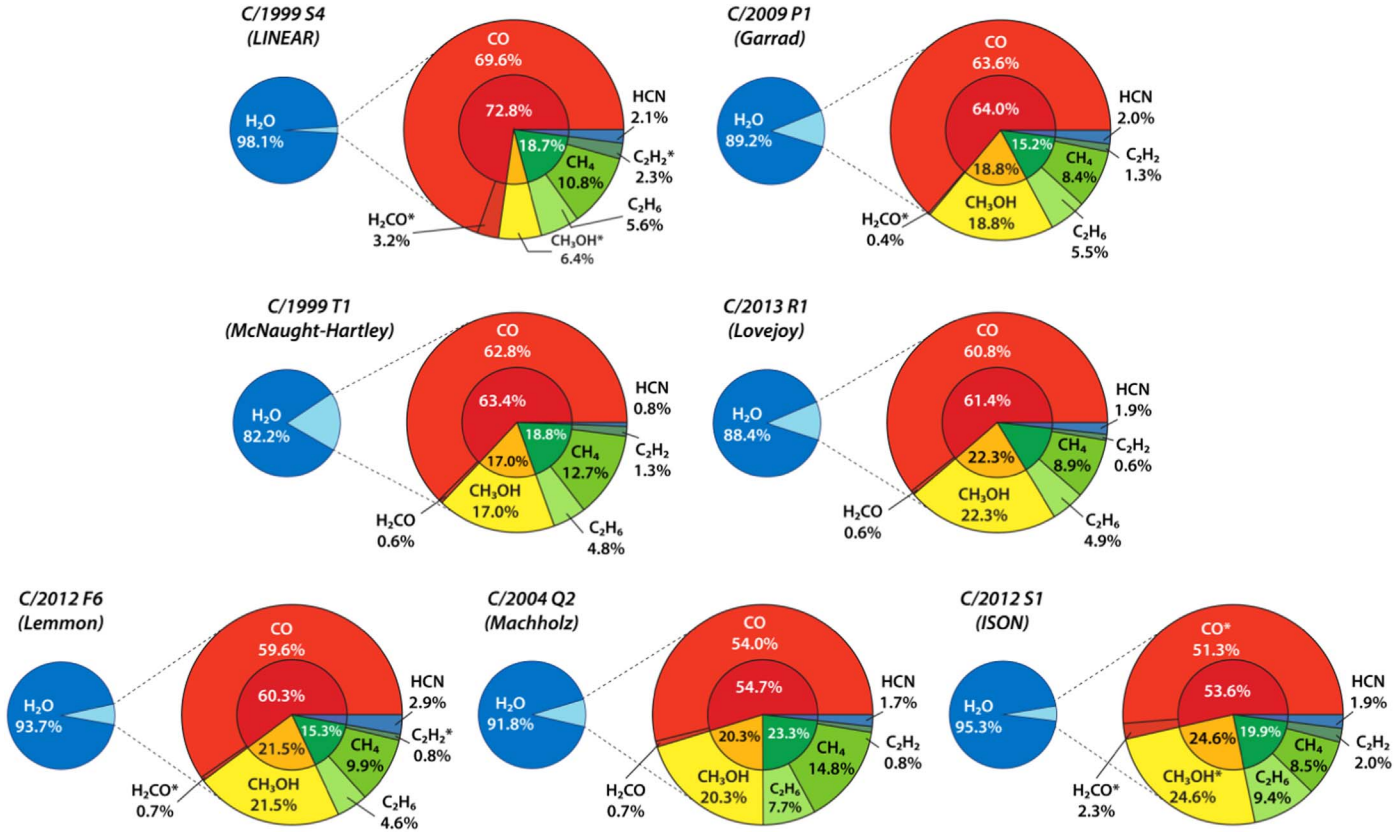

Figure 4. First group of two-level pie charts ordered with decreasing CO. Different colors indicate different functional groups, as described in Section 3.2. For each comet, the reported proportions are obtained by normalizing the MRs to their sum. Starred labels represent 2σ upper limits.

comets, HCN always shows a lower value with respect to ammonia; this could be the signature of formation of ammonium cyanide salt on grains in regions where NH_3 formation exceeds that of HCN (Mumma et al. 2019; Altwegg et al. 2020; Poch et al. 2020). Comets in the second group display comparable to higher amounts of NH_3 with respect to C_2H_6 and CH_4 and in some cases show some of the highest proportions for this molecule (see, for example, comets 8P and 9P); exceptions to this rule are comets C/2007 N3 and C/2001 A2, which instead show a very low amount of ammonia. Also in this case, we observe, on average, higher proportions of ammonia with respect to HCN, except for 73P. On the other side, HCN proportions in the second group tend to be higher with respect to those of the same species in the first group.

3.3. Correlation Analysis

3.3.1. Correlations between Single MRs

In Table 5, we report the Spearman rank-order correlation factors (ρ_{Sp}) and corresponding statistics, two-sided level of significance (p-value, p), and degrees of freedom (df = number of measures minus 2) for each combination of the studied molecular species. In Figure 7 we show four examples. We have chosen the Spearman correlation because it corresponds to the nonparametric version of the Pearson product–moment correlation, and, in general, it assesses how well the relationship between two variables can be described using a monotonic function, not necessarily linear. When the relationship between the two variables is linear, the Spearman correlation factor should correspond with the Pearson value. The values reported in Table 5 were calculated using the MRs reported in Table 2; to improve our statistics, we included in the computation the most significant 2σ upper limits, i.e., upper limits lower than the 25th percentile from the box plot statistic.

From Table 5, it is possible to notice that the hydrocarbon pairs C_2H_6–CH_4, CH_4–C_2H_2, and C_2H_6–C_2H_2 all show a high value of the Spearman correlation factor (0.89, 0.79, and 0.85, respectively), suggesting a potential common origin for these molecules. The MRs of methanol also show high ρ_{Sp} if paired with methane, ethane, and acetylene (0.73, 0.85, and 0.65, respectively). Correlation factors between hydrocarbons and MRs of CO range from about 0.5 for C_2H_6 to about 0.7 for C_2H_2 and 0.8 for CH_4; CO also shows a medium Spearman correlation factor in combination with CH_3OH and NH_3 (about 0.5) similar to the one between NH_3 and C_2H_2. A slight trend exists between the relative MRs of H_2CO–CH_4 and H_2CO–CH_3OH (about 0.4). Other combinations of MRs do not show correlations or anticorrelations with values higher than these numbers.

If we compare our Spearman correlation factors with the Pearson correlation values reported in Dello Russo et al. (2016), we do not see any strong parallels, except for some similarities in the relationships observed among hydrocarbons and for the combination of CH3OH with NH3 and CH3OH with hydrocarbons. In particular, we do not observe the high positive correlations previously found between HCN and hydrocarbons. While the previous findings are consistent with the high positive correlation seen between CN and C_2 in optical databases (A'Hearn et al. 1995; Cochran et al. 2012), our correlation factors are not consistent with this hypothesis. These differences are in part expected, since we are using different data sets and a different approach to retrieve these factors.

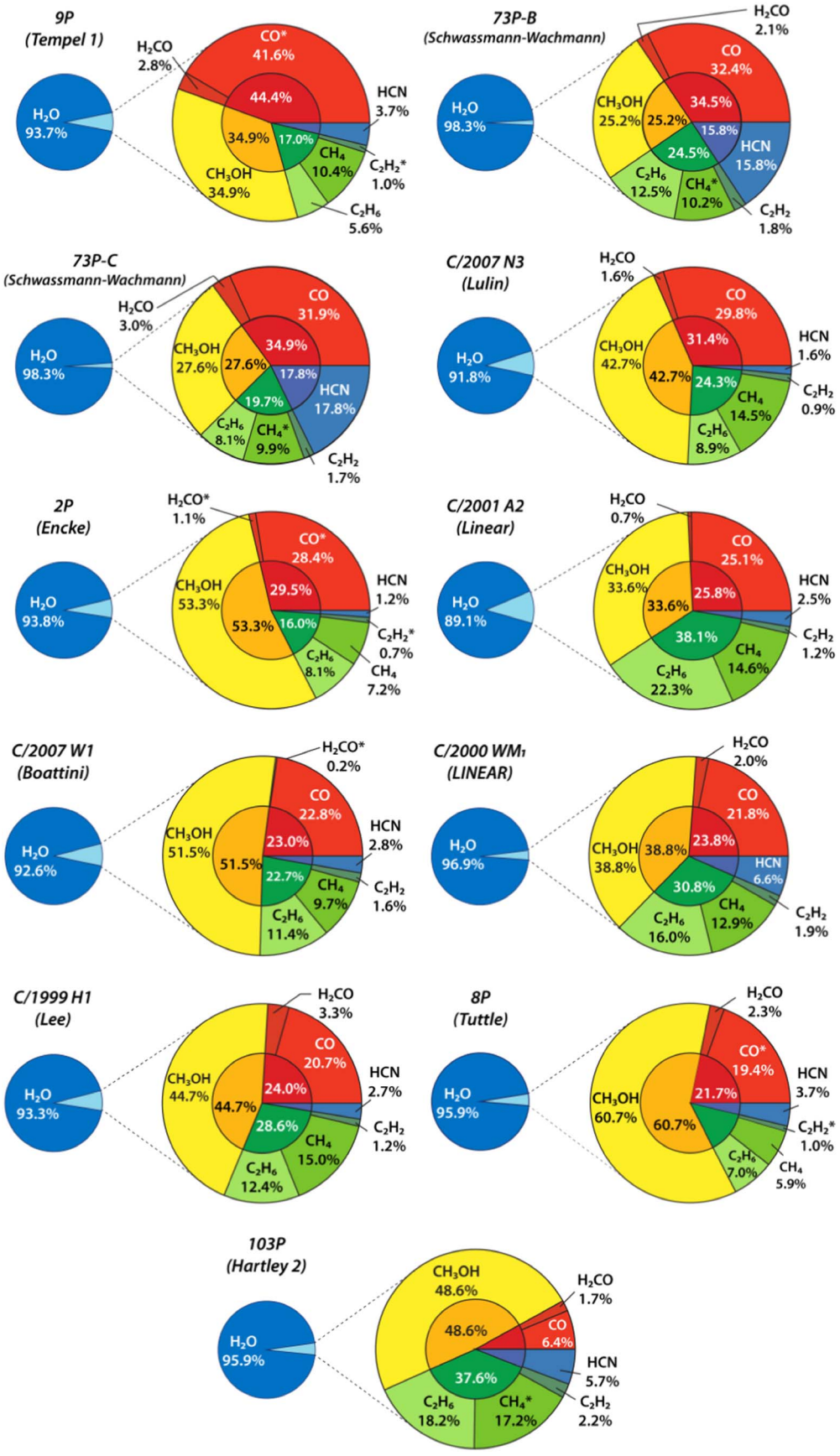

Figure 5. Second group of two-level pie charts ordered with decreasing CO. See Figure 4 for a description.

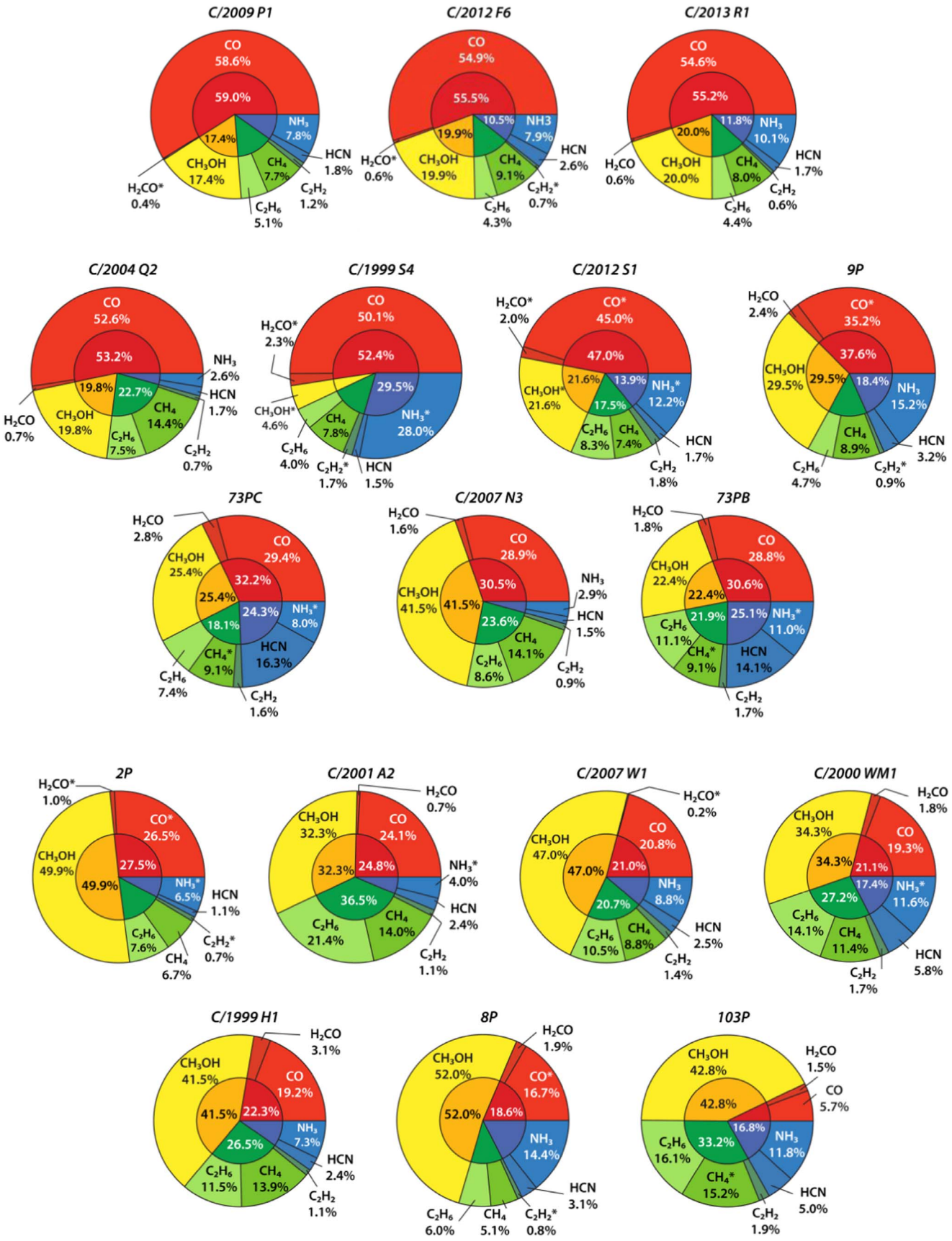

Figure 6. Two-level pie charts obtained including NH_3, ordered with decreasing CO. See Figure 4 for a description.

Table 5
Spearman's Correlations among the Updated MRs[a]

	CH_3OH	HCN	NH_3	H_2CO	C_2H_2	C_2H_6	CH_4	CO
CH_3OH	...	0.19 0.43 18	0.32 0.21 15	0.38 0.15 14	0.65 0.002 18	**0.85** **2×10^{-6}** **18**	0.73 9×10^{-4} 15	**0.52** **0.05** **13**
HCN	...	...	0.05 0.86 15	−0.30 0.26 14	0.20 0.40 18	**0.26** **0.27** **18**	0.01 0.97 15	−0.10 0.71 13
NH_3	...	...	...	0.18 0.54 12	0.47 0.06 15	0.18 0.49 15	0.23 0.42 12	0.57 0.04 11
H_2CO	...	...	...	...	0.22 0.40 14	0.29 0.27 14	0.40 0.14 13	0.14 0.63 12
C_2H_2	...	...	...	...	...	0.85 2×10^{-6} 18	0.80 1×10^{-4} 15	0.62 0.01 13
C_2H_6	...	...	...	...	...	...	**0.89** **2×10^{-6}** **15**	0.45 0.09 13
CH_4	...	...	...	...	...	...	...	0.79 0.001 11
CO	...	...	...	...	...	...	...	...

Note.
[a] The first value in each cell is the Spearman correlation coefficient (ρ_{Sp}) calculated including 2σ upper limits below the 25th percentile; below each correlation coefficient, we report the two-sided level of significance (p) and the degrees of freedom of the calculation (df). Cells in bold are shown in Figure 7.

3.3.2. Correlations between Ratios of MRs and Their Relationships with Orbital Parameters

Based on the distribution of molecular species in comets inferred through the pie charts, we investigated the interrelationships among ratios of MRs relative to six selected molecular species (CH_3OH, CO, NH_3, C_2H_6, HCN, and CH_4). The retrieved Spearman correlation factors ρ_{Sp} and corresponding statistics, determined as described in Section 3.3.1 and Appendix B, are reported in Table 6. To improve the statistics, we included in the computation the most significant 2σ upper limits (i.e., upper limits lower than the 25th percentile value from the box plot statistic). Hereafter, we describe three selected cases, which we illustrate in Figures 8–10; other correlations among three and four species combinations are under study, and a more detailed analysis will be given elsewhere.

In Figure 8, we show the relationships between MR(CH_3OH)/MR(CO) (hereafter CH_3OH/CO) and MR(C_2H_6)/MR(CH_4) (hereafter C_2H_6/CH_4), along with the corresponding graphs of these two ratios with respect to the Tisserand invariant, the perihelion distance, and the inclination of the orbit. The colors scale with the values of the Tisserand invariant ($-2 < T_J < -0.6$, red; $-0.6 < T_J < 0.6$, yellow; $0.6 < T_J < 2$, green; $T_J > 2$, blue).

It is possible to tentatively group our comet sample in the following way.

Group 1: C/1999 H1 and C/2007 N3, comets that have $-2 < T_J < -0.6$. They both show MRs of CH_3OH higher than those of CO and C_2H_6 lower than those of CH_4, being characterized at the same time by a high inclination.

Group 2: C/2009 P1, C/2012 F6, C/1999 T1, and C/2013 R1, comets that have low values for both the CH_3OH/CO and C_2H_6/CH_4 ratios and $-0.6 < T_J < 0.6$, with perihelion distances between about 0.6 and 1.6 au and medium-to- high inclinations.

Group 3: C/2001 A2 and C/2007 W1, comets that have $0.6 < T_J < 2$, a perihelion distance from about 0.7 to 1 au, and inclinations lower than 50°. These comets show high values for both the CH_3OH/CO and C_2H_6/CH_4 ratios.

Exceptions to this grouping are comet C/2000 WM_1 (yellow/green), which acts as the third group even if its orbital parameters are similar to the second group, and comet C/2004 Q2 (yellow/green), which shows many similarities with the second group even if it is dynamically more like the third group. Comet C/1999 S4 (red/yellow) has orbital parameters similar to those of C/1999 H1 and C/2007 N3 (group 1) but seems to behave like comets in the second group; however, the very low upper limit retrieved for CH_3OH suggests that this comet may be a kind of its own. Indeed, it is not possible to infer from our data set if these three comets represent a transition between different groups or different groups by themselves. The JF comets ($2 < T_J < 3$) show a spread of the two different ratios, but the majority of CH_4 and CO MRs correspond to 2σ upper limits, so it is not possible to properly constrain their nature considering only our data set. Nevertheless, from panel (a), it looks like comet 9P locates between groups 1 and 2, while 73P falls between groups 2 and 3. Comets 2P and 103P are more compatible with group 3, with

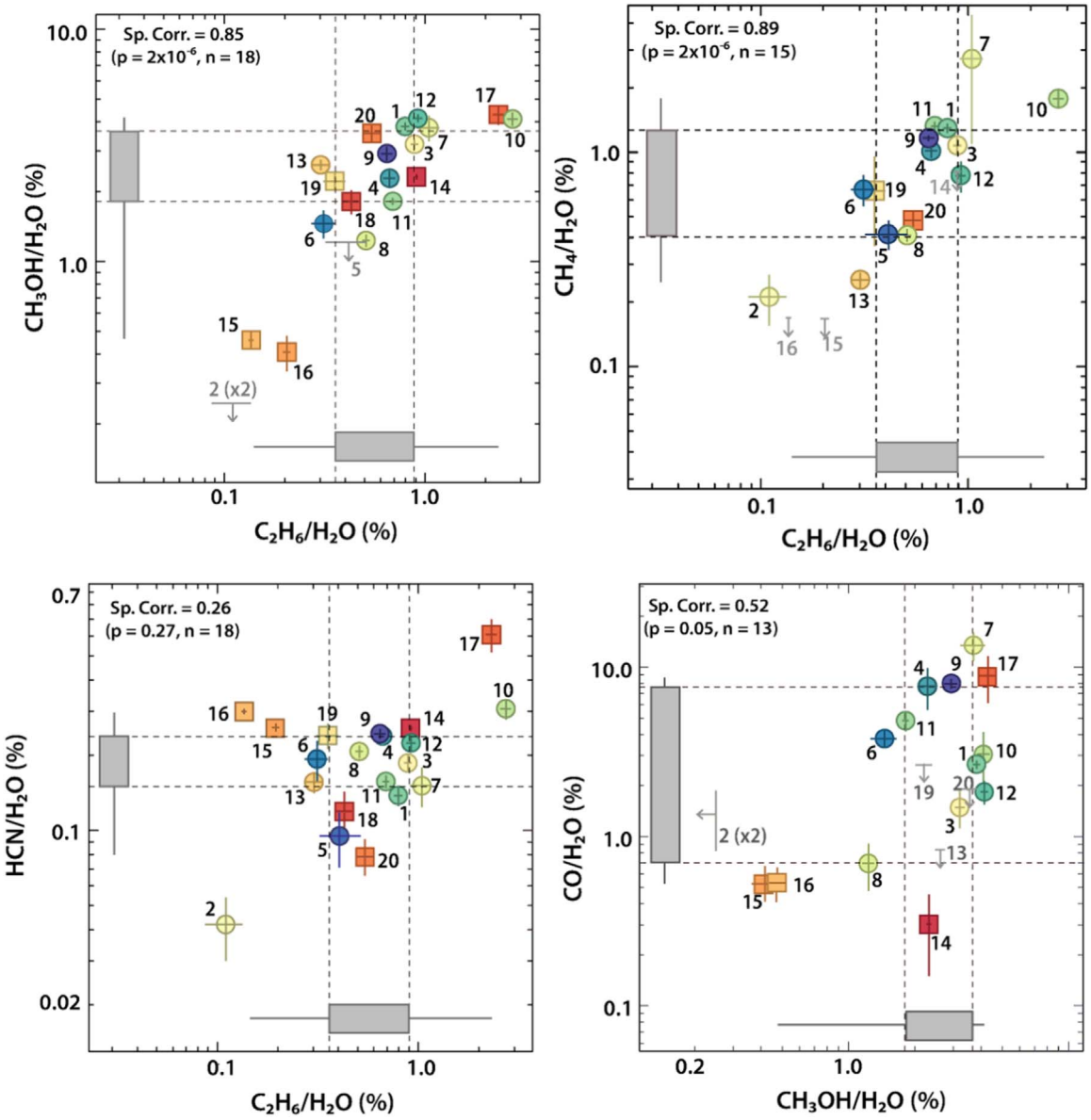

Figure 7. Examples of correlations among the different molecular species observed in our sample of comets. In each panel, the circles indicate OC comets, and the squares indicate JF comets, while 2σ upper limits are shown as gray arrows and tags for comparison. Spearman's correlation coefficients and corresponding statistics are reported in the upper left corner of each panel. Box plot statistics are shown for each axis. The data are numbered following the increasing Tisserand invariant (see Table 1).

103P particularly depleted in CO. The Halley-type comet 8P also appears to fit group 3.

If we substitute HCN for CH_3OH, we obtain very similar tendencies, as shown in Figure 9; in particular, comets in group 2 show lower values of MR(HCN)/MR(CO) (hereafter HCN/CO) with respect to comets in group 3. In this case, comet C/1999 H1 seems to differ from C/2007 N3 and C/1999 S4 (even so, we kept the color codes used in the previous figure). Comets with a Tisserand parameter $T_J > 2$ may group as follows: 9P remains in a similar location as before (between groups 1 and 2), 2P tends toward the third group, while comets 103P and 73P seem to form a group by themselves, with HCN much enhanced with respect to CO.

Finally, in Figure 10, we tested $MR(CH_3OH)/MR(NH_3)$ versus $MR(HCN)/MR(C_2H_6)$ (hereafter CH_3OH/NH_3 and HCN/C_2H_6, respectively), which shows a negative correlation but a similar clustering of comets, with C/2009 P1, C/2012 F6, and C/2013 R1 showing high HCN/C_2H_6 coupled with low CH_3OH/NH_3 abundance ratios, and comets in the first and third groups displaying a slightly opposite behavior. In this case, it was also possible to include more JF comets in this analysis; even if the ratios for these comets agree with the negative correlation trends of the OC comets seen in panel (a), the relative ratios of MRs with respect to their orbital parameters do not seem to follow any rule, and their values are spread quite widely, especially considering the HCN/C_2H_6 ratio. Nevertheless, 103P seems to match with group 3 and 9P with group 2. The spreading of the different combinations of molecules that we find among comets with $T_J > 2$ for all three examples is potentially related to the different histories that these same comets experienced during their life and, most likely, to the loss of the hypervolatile material during multiple passages in the inner solar system.

Table 6
Spearman Correlations among Ratios of the Updated MRs[a]

	$\frac{CH_3OH}{HCN}$	$\frac{CH_3OH}{NH_3}$	$\frac{CH_3OH}{C_2H_6}$	$\frac{CH_3OH}{CH_4}$	$\frac{CH_3OH}{CO}$	$\frac{HCN}{NH_3}$	$\frac{HCN}{C_2H_6}$	$\frac{HCN}{CH_4}$	$\frac{HCN}{CO}$	$\frac{NH_3}{C_2H_6}$	$\frac{NH_3}{CH_4}$	$\frac{NH_3}{CO}$	$\frac{C_2H_6}{CH_4}$	$\frac{C_2H_6}{CO}$	$\frac{CH_4}{CO}$
$\frac{CH_3OH}{HCN}$	…	*0.49* *0.05* *15*	*0.58* *0.007* *18*	*0.40* *0.14* *13*	*0.18* *0.53* *13*	*−0.56* *0.02* *15*	*−0.76* *1 × 10^{-4}* *18*	*−0.49* *0.06* *13*	*−0.38* *0.17* *13*	−0.16 0.54 15	−0.27 0.39 10	−0.18 0.55 11	0.24 0.39 13	0.03 0.91 13	0.34 0.31 9
$\frac{CH_3OH}{NH_3}$	…	…	*−0.10* *0.72* *15*	*0.01* *0.97* *10*	*0.48* *0.10* *11*	*0.37* *0.15* *15*	**−0.77** ***3 × 10^{-3}*** **15**	−0.69 0.01 10	0.07 0.81 11	*−0.85* *1 × 10^{-6}* *15*	*−0.73* *0.007* *10*	*−0.29* *0.34* *11*	0.35 0.27 10	0.43 0.14 11	0.62 0.08 7
$\frac{CH_3OH}{C_2H_6}$	…	…	…	*0.64* *0.01* *13*	*0.11* *0.69* *13*	−0.70 0.002 15	*0.02* *0.95* *18*	0.19 0.49 13	−0.19 0.49 13	*0.54* *0.03* *15*	0.45 0.14 10	−0.06 0.84 11	*−0.01* *0.96* *13*	*−0.25* *0.38* *13*	−0.06 0.85 9
$\frac{CH_3OH}{CH_4}$	…	…	…	…	*0.91* *1 × 10^{-5}* *9*	−0.54 0.07 10	0.12 0.68 13	*0.48* *0.07* *13*	0.77 *0.005* 9	0.33 0.30 10	*0.57* *0.05* *10*	0.80 0.01 7	*0.68* *0.006* *13*	0.72 0.01 9	*0.58* *0.06* *9*
$\frac{CH_3OH}{CO}$	…	…	…	…	…	0.04 0.89 11	−0.17 0.55 13	0.25 0.45 9	*0.81* *3 × 10^{-4}* *13*	−0.46 0.11 11	−0.13 0.73 7	*0.68* *0.01* *11*	**0.74** **0.01** **9**	*0.90* *4 × 10^{-6}* *13*	*0.78* *4 × 10^{-4}* *9*
$\frac{HCN}{NH_3}$	…	…	…	…	…	…	*0.09* *0.74* *15*	*−0.36* *0.25* *10*	*0.46* *0.12* *11*	*−0.62* *0.009* *15*	*−0.78* *0.003* *10*	*−0.18* *0.57* *11*	0.06 0.82 10	0.16 0.60 11	0.45 0.22 7
$\frac{HCN}{C_2H_6}$	…	…	…	…	…	…	…	*0.82* *2 × 10^{-4}* *13*	*0.29* *0.30* *13*	*0.70* *0.002* *15*	0.68 0.02 10	0.32 0.29 11	*−0.19* *0.51* *13*	*−0.19* *0.51* *13*	−0.39 0.23 9
$\frac{HCN}{CH_4}$	…	…	…	…	…	…	…	…	*0.41* *0.21* *9*	0.68 0.02 10	*0.79* *0.002* *10*	0.72 0.03 7	*0.36* *0.19* *13*	0.18 0.59 9	*−0.09* *0.79* *9*
$\frac{HCN}{CO}$	…	…	…	…	…	…	…	…	…	−0.14 0.64 11	−0.08 0.83 7	*0.74* *0.004* *11*	**0.77** ***0.005*** **9**	*0.80* *3 × 10^{-4}* *13*	*0.83* *0.002* *9*
$\frac{NH_3}{C_2H_6}$	…	…	…	…	…	…	…	…	…	…	*0.87* *2 × 10^{-4}* *10*	*0.26* *0.39* *11*	*−0.29* *0.37* *10*	*−0.57* *0.04* *11*	−0.60 0.09 7
$\frac{NH_3}{CH_4}$	…	…	…	…	…	…	…	…	…	…	…	*0.63* *0.07* *7*	*0.17* *0.60* *10*	−0.20 0.61 7	*−0.30* *0.43* *7*
$\frac{NH_3}{CO}$	…	…	…	…	…	…	…	…	…	…	…	…	0.62 0.08 7	*0.62* *0.02* *11*	*0.47* *0.21* *7*

Table 6
(Continued)

	$\frac{CH_3OH}{HCN}$	$\frac{CH_3OH}{NH_3}$	$\frac{CH_3OH}{C_2H_6}$	$\frac{CH_3OH}{CH_4}$	$\frac{CH_3OH}{CO}$	$\frac{HCN}{NH_3}$	$\frac{HCN}{C_2H_6}$	$\frac{HCN}{CH_4}$	$\frac{HCN}{CO}$	$\frac{NH_3}{C_2H_6}$	$\frac{NH_3}{CH_4}$	$\frac{NH_3}{CO}$	$\frac{C_2H_6}{CH_4}$	$\frac{C_2H_6}{CO}$	$\frac{CH_4}{CO}$
$\frac{C_2H_6}{CH_4}$	…	…	…	…	…	…	…	…	…	…	…	…	…	*0.95* *1×10^{-5}* *9*	*0.59* *0.06* *9*
$\frac{C_2H_6}{CO}$	…	…	…	…	…	…	…	…	…	…	…	…	…	…	*0.77* *0.005* *9*
$\frac{CH_4}{CO}$	…	…	…	…	…	…	…	…	…	…	…	…	…	…	…

Note.
[a] See Table 5 for a description. The ratios in the first row and column are the ratios of MRs relative to water. Correlations that have the same molecular species in the numerator or denominator are shown in italic. Cells in bold are shown in Figures 8–10 and discussed in the text.

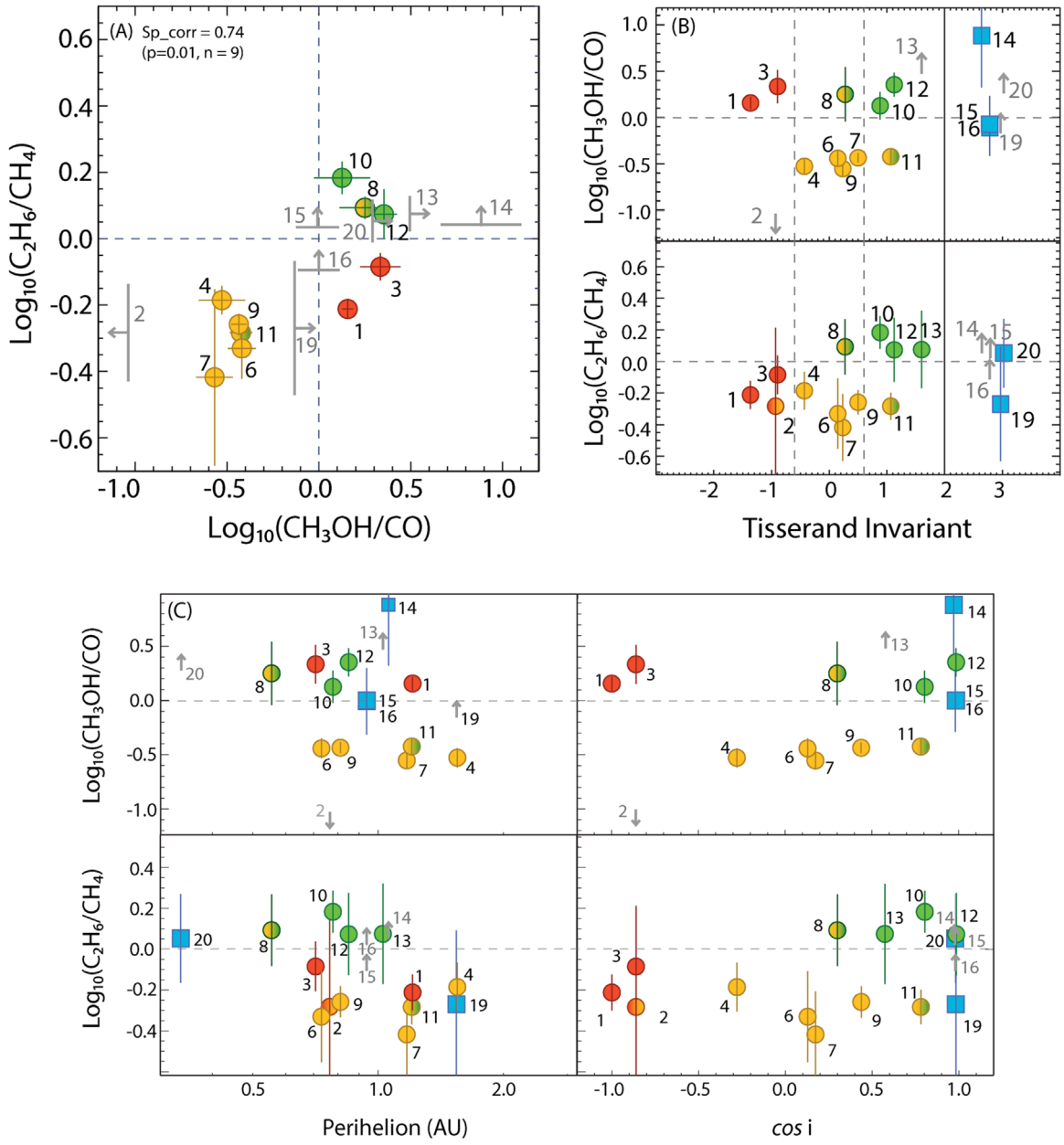

Figure 8. Comparison between (a) the MR(CH_3OH)/MR(CO) and MR(C_2H_6)/MR(CH_4) ratios (indicated in the plot as CH_3OH/CO and C_2H_6/CH_4, respectively), (b) the same ratios as a function of the Tisserand invariant, and (c) the same ratios as a function of the perihelion distance and orbit inclination. In each panel, 2σ upper limits are shown with gray arrows and tags. In panel (a), we report the Spearman correlation factor and its statistic. Colors and numbers are given following the increasing Tisserand invariant and considering possible clusters related to different chemical compositions, as described in the text.

The previous three examples agree and improve the classification produced using the pie charts, showing that in principle, it may be possible to relate the chemical composition of comets to their dynamical properties. Our tentative classification shows only a few similarities with the one presented by Dello Russo et al. (2016); nevertheless, our sample is still small to reach firm conclusions.

3.4. Testing the Origins and Chemical Evolution of Comets

Some of the distributions and correlations that we observed in our sampled comets may be consistent with recent theories of molecular formation in protoplanetary disks, where the chemistry is driven mainly by both the temperature gradient and the radiation fields produced by the forming star and the external environment (see, for example, Walsh et al. 2010; Eistrup et al. 2016, 2018; Bosman et al. 2018; Pontoppidan et al. 2019).

For example, carbon monoxide should be in the gas phase in the inner part of the disk midplane, where temperatures are warmer than its sublimation temperature ($T > 26$ K) and it can react with other molecules and/or radicals to form more complex species, like, for example, CO_2 (Furuya & Aikawa 2014; Schwarz et al. 2018). At the same time, some preservation mechanisms of interstellar CO can be active when the gas is mixed through the midplane, and at every vertical cycle, some of these molecules may freeze out onto grains and not cycle back to the gas (Kama et al. 2016); this may explain very high abundances of CO in some comets. Conversely, in regions of the disk where the temperatures drop below 26 K, hydrogenation on grain surfaces is thought to become the

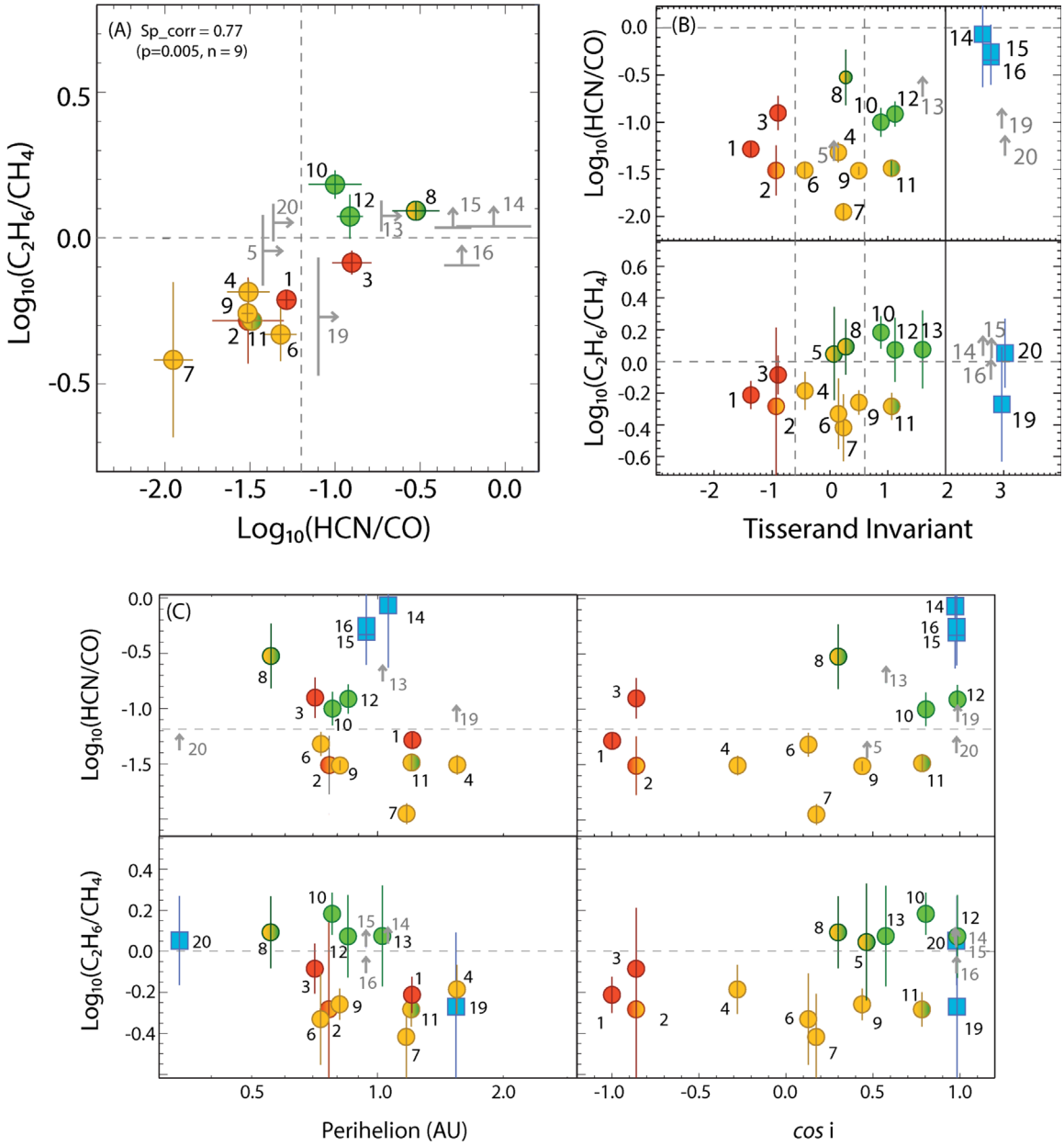

Figure 9. Same as Figure 8 but with MR(HCN)/MR(CO) and MR(C_2H_6)/MR(CH_4) (indicated in the plot as HCN/CO and C_2H_6/CH_4, respectively).

dominant chemical process, and CO can be efficiently converted to other species, such as CH_3OH (Hiraoka et al. 2005). Being among the most volatile species, CO is also more likely to be lost during the lifetime of a comet due to heating of the nucleus surface as the comet experiences repeated passages through the inner solar system; this is particularly true for JF comets. These diverse formative and evolutionary scenarios are compatible with the broad range of MR values that we measure for this molecule while also considering that the original information on CO abundances in some comets may have changed over time.

Methanol is the least volatile species among the analyzed trace gases, and it shows a less extended distribution compared with CO. It has no known efficient gas-phase formation route (Garrod & Herbst 2006; Geppert et al. 2006), but it should form efficiently on grains starting from hydrogenation of CO (Hidaka et al. 2004) and be abundant in those comets that formed in regions of the disk beyond the CO snow line. Recent studies (Qasim et al. 2018) suggest that CH_3OH formation is also possible during earlier phases of interstellar ice evolution through the sequential surface reaction chain, $CH_4 + OH \rightarrow CH_3 + H_2O$ and $CH_3 + OH \rightarrow CH_3OH$, at 10–20 K in H_2O-rich dense regions. Methanol is much less volatile than CO, and its abundances are not expected to change much over the lifetime of a comet.

Hydrocarbons could build up from successive H-atom additions to the products of other photodissociated molecules. Methane may form from successive hydrogenation of photo-products (C, CH_2, CH_3) and accumulate in the ice form in the outer disk, beyond its snow line. Later in time, when the dust begins to agglomerate and energetic radiation penetrates more efficiently into the disk, C_2H_6 can also be produced via recombination of the photodissociation products of methane (e.g., CH, CH_2, and CH_3; see, for example, the disk chemical evolution described in Bosman et al. 2018 or Eistrup et al. 2018).

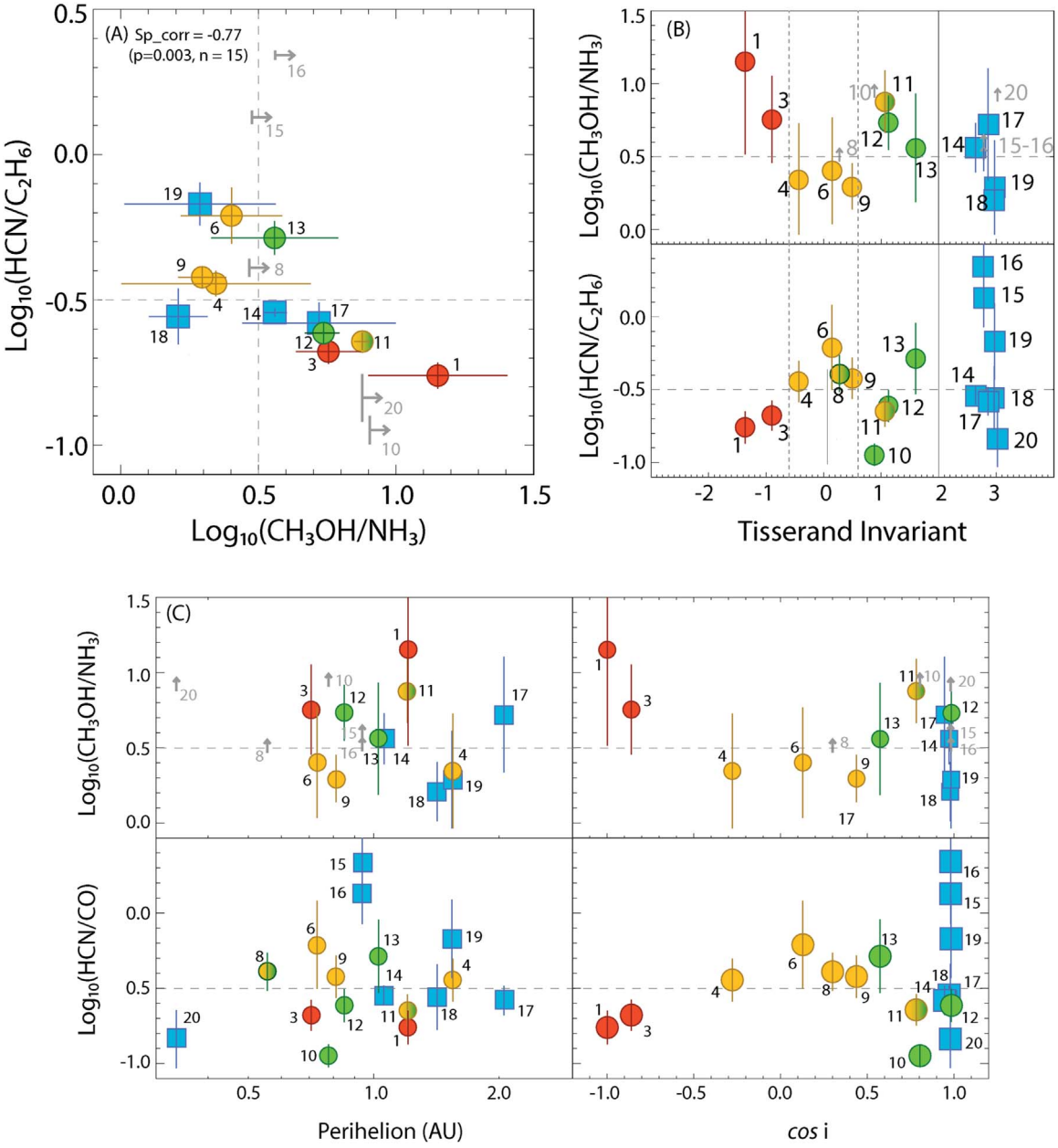

Figure 10. Same as Figure 8 but with MR(CH_3OH)/MR(NH_3) and MR(HCN)/MR(C_2H_6) (indicated in the plot as CH_3OH/NH_3 and HCN/C_2H_6, respectively).

If so, we might expect some comets with high C_2H_6/CH_4 ratios, as, for example, comets in group 3. In addition, ethane can also form from hydrogenation of C_2H_2 (Hiraoka et al. 2000) and accumulate beyond the C_2H_6 snow line and within the CH_4 snow line. The lower median value measured for acetylene with respect to C_2H_6 in our sample may reflect this process. An alternative path for hydrocarbon formation could be through destruction of polycyclic aromatic hydrocarbons in the molecular layer and successive freezing onto grains (Tielens 2013); this may also explain in part the high positive correlations that we observe among hydrocarbons.

Following Schwarz & Bergin (2014), ammonia may form from successive hydrogenation of NH and can be abundant already at 5 au; the compact distribution that we see in Figure 2 agrees with a common value shared among the comet population. This is true except for C/2004 Q2 and C/2007 N3, which show strongly depleted values compared to the other comets. The reason for this enhanced depletion in these two comets is not clear; however, NH_3 may be easily incorporated into ammonium salts through reactions with organic acids on grains, even at temperatures well below 30 K, thereby limiting the abundance of free NH_3 that can be retained as a primary volatile in comets (Mumma et al. 2019; Altwegg et al. 2020; Poch et al. 2020). The search for by-products of ammonium salts in the coma of active comets is expected to provide new insights on nitrogen chemistry in the coming years. The HCN should form instead via gas-phase reactions in warmer regions and then be quickly adsorbed onto the grains; in colder regions, the nitrogen is more likely to take part in the formation of NH_3 than HCN, so that the latter will show a more dispersed distribution in the comet population and a lower median value.

Finally, H_2CO is among the species that show the lowest abundances in our study, probably related to formaldehyde as an intermediate product in the formation of CH_3OH from

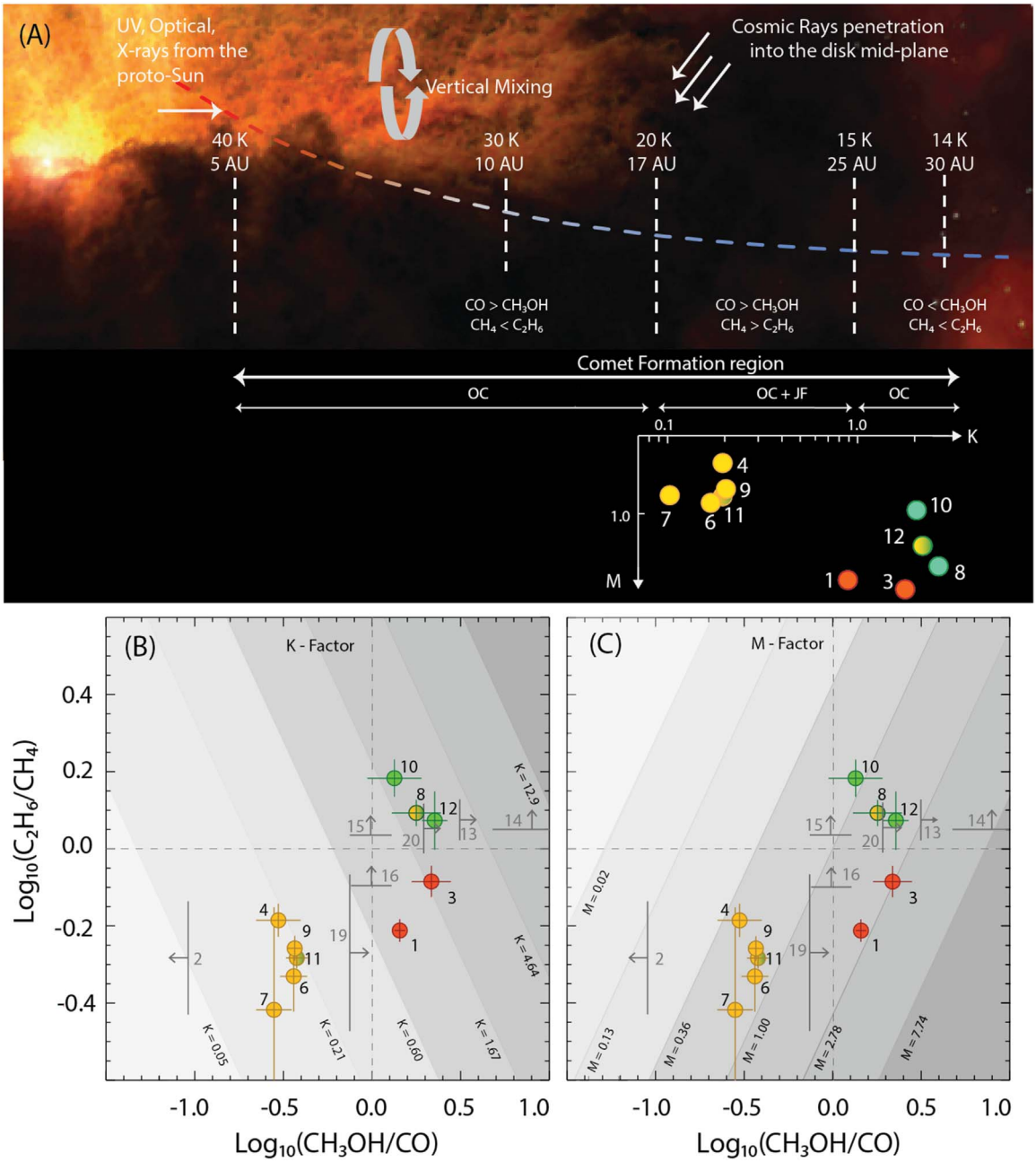

Figure 11. Connections between protoplanetary disks and comets. In the upper panel, we illustrate a scheme of the disk showing some of the major chemical–physical processes that involve the material that will be incorporated into cometary nuclei. Below the disk, we tentatively locate comets from our sample, following the discussion in the text (only comets with determined values for CH_3OH, CO, C_2H_6, and CH_4 are shown). In panels (b) and (c), we show the relationships between the $MR(CH_3OH)/MR(CO)$ and $MR(C_2H_6)/MR(CH_4)$ ratios (indicated in the plot as CH_3OH/CO and C_2H_6/CH_4, respectively), and we report a selection of the bundle of straight lines $K = (MR(CH_3OH) \times MR(C_2H_6))/(MR(CH_4) \times MR(CO))$ (panel (b)) and $M = (MR(CH_3OH) \times MR(CH_4))/(MR(C_2H_6) \times MR(CO))$ (panel (c)), which we show in gray scale.

hydrogenation of CO. The depletion of the H_2CO monomer may also be related to sequestration in the form of polymeric formaldehyde, as was inferred from mass spectral measurements in comet Halley and spectral mapping of other comets (Meier et al. 1993; Cottin & Fray 2008).

Considering the relationship between $MR(CH_3OH)/MR(CO)$ and $MR(C_2H_6)/MR(CH_4)$, we searched for potential links with the chemistry predicted in different disk regions where comets may have formed (see Figure 11). We mainly followed the disk model described in Bosman et al. (2018), where the authors explained the depletion of CO observed with the Atacama Large Millimeter/submillimeter Array in a large portion of protoplanetary disks as the result of the spatial and temporal evolution of CO in molecules such as CH_3OH, CH_4, and C_2H_6 (similar considerations can be found in Walsh et al. 2010; Eistrup et al. 2016, 2018). A general discussion should consider the positions of the molecular "snow lines" as a function of the luminosity of the central star (e.g., T Tauri versus HAe disks; Walsh et al. 2015; Wei et al. 2019) and the evolutionary stages of the disks (Garaud & Lin 2007; Oka et al. 2011; Piso et al. 2015; Ruaud & Gorti 2019). Here, as a simplification, we will assume that the CH_4 snow line locates at about 17 au, while the CO snow line locates at 25 au; these are considered "typical" midplane temperature profiles for a

disk around a solar-mass star (Bergin & Cleeves 2018 and references therein). We can identify four different scenarios.

1. *Comets that formed between 5 au and the methane snow line (assumed at about 17 au).* This region should reflect a chemistry dominated by gas-phase processes, and it corresponds to the region where some of the OC comets formed (Levison & Morbidelli 2003; Gomes et al. 2005). In this region, CO is mainly gaseous, even if it can be trapped in ice form in dust grains (Kama et al. 2016). An efficient gas-phase formation route for CO conversion to methanol is lacking (Geppert et al. 2006), so the latter is expected to be scarce. At temperatures of a few hundred kelvins, the C^+ channel can produce gas-phase CH_4 (Aikawa et al. 1999), which can be successively destroyed via photodissociation by cosmic-ray-induced photons, in favor of CO_2 and/or unsaturated hydrocarbons, such as gas-phase C_2H_4. Ethylene will, in turn, freeze onto grains and be hydrogenated to ethane, which may become abundant (Dodson-Robinson et al. 2018). A comet formed in this region may show MRs of CH_3OH lower than those of CO and MRs of C_2H_6 higher than those of methane, which would place it in the upper left quadrant of the graph in Figures 11(b) and (c). None of the comets presented in this paper fall into this scenario.
2. *Comets that formed between the methane and CO snow lines (between about 17 and 25 au).* Both OC and JF comets may have formed in this region of the disk. As in case 1, CO is still mainly in the gas state, and CH_3OH is not forming efficiently. On the other hand, behind its snow line, CH_4 will freeze and be abundant on grains, and C_2H_6 will not form efficiently through hydrogenation of the photodissociation products of CH_4. Comets formed in this region are expected to be characterized by MRs of CO higher than those of CH_3OH and MRs of CH_4 higher than those of C_2H_6. That would place them in the lower left quadrant of the graphs. Comets like C/1999 S4, C/2013 R1, C/2012 F6, and C/2004 Q2 fall into this region, and they all show a ratio $MR(CH_4):MR(C_2H_6) \sim 2:1$. Comets C/2009 P1 and C/1999 T1 also show a high CH_4/C_2H_6 ratio coupled with a high amount of CO; this may suggest a possibly different origin for these comets or highly efficient preservation mechanisms for CO and CH_4 in some of the comets formed in this region.
3. *Comets that formed beyond the CO snow line (at distances larger than 25 au) during the early stages of the disk.* Comets that formed in this region (some of the OC comets) should carry signatures of hydrogenation on grain surfaces. Following Bosman et al. (2018), the final product of successive hydrogenations of CO is CH_3OH, which will be particularly enriched in the early stage of the disk lifetime (the first 3 Myr). Methanol is then expected to be photoprocessed in favor of CH_4, which will become one of the most abundant hydrocarbons after 5 Myr. Comets that formed in this region before 5 Myr will show relative abundances of CO lower than methanol and $MR(CH_4) > MR(C_2H_6)$, and they should be located in the lower right quadrant of the graph in Figures 11(b) and (c) (in our sample, comets C/2007 N3 and C/1999 H1).
4. *Comets that formed beyond the CO snow line (at distances larger than 25 au) in a later stage of the disk.* After about 5 Myr, methane will decrease in favor of C_2H_6 (Bosman et al. 2018). Some of the comets that formed at distances >25 au and collected processed material that formed later in time may show $MR(CH_4) < MR(C_2H_6)$ and therefore be located in the upper right quadrant (C/2001 A2, C/2000 WM_1, and C/2007 W1). In this group, we may also include comets that could have incorporated material coming from the molecular layer, where the chemistry of hydrocarbons is much enhanced (Schwarz et al. 2018).

The spread in locations for JF comets probably results from both the original composition and the loss of the most volatile species during multiple revolutions around the Sun, along with the lack of precise measurements of CH_4 and CO for this dynamical family.

If we consider the bundle of straight lines $K = (MR(CH_3OH) \times MR(C_2H_6))/(MR(CH_4) \times MR(CO))$ (see Figure 11(b)), we can associate an increasing K with the increasing formation distance of the comet from the proto-Sun (mainly for long-period comets) and/or to postformation evolution of the cometary material (mainly but not only for short-period comets). In fact, we expect a higher contribution of CH_3OH and C_2H_6, especially for those comets where hydrogenation processes were efficient (low temperatures). In this way, we can assume, for example, that comets like C/1999 S4, C/2013 R1, and C/2009 P1 probably formed closer to the proto-Sun, while comets like C/2001 A2, C/2000 WM_1, and C/2007 W1 formed at larger distances, beyond the CO snow line; these comets may also have incorporated material that formed in a late stage of the protoplanetary disk evolution.

In a similar way, if we trace the lines $M = (MR(CH_3OH) \times MR(CH_4))/(MR(C_2H_6) \times MR(CO))$ (see Figure 11(c)), we can associate with each comet a second factor, whose value could be indicative of a processing of material by UV/X-ray/cosmic-ray radiation and successive H-atom addition during a later stage of the disk, with a lower value of M indicative of high efficiency in this process. Considering our sample, for example, C/2000 WM_1, C/2007 W1, and C/2001 A2 share about the same K, but the lower value for M in C/2001 A2 suggests that the material in this comet may have experienced higher photolysis. The K and M factors are reported in Table 7.

4. Conclusions and Future Steps

We presented updated MRs (% with respect to water) for 20 comets observed with NIRSPEC at the Keck Observatory since 1999. The results were obtained using full quantum molecular models and the latest analysis techniques available to our group. We performed a descriptive statistic and correlation analysis on these results, trying to connect the abundances observed in these comets to the possible origin and evolution of the material in the protoplanetary disk.

Our analysis reveals that the composition of comets reflects a combination of chemical–physical processes (e.g., radical–radical reactions, hydrogenation, vertical mixing) that influenced the different portions of the disk midplane over time. Moreover, modification of the surface material of a nucleus after its formation may occur, especially for short-period comets.

We identified two main chemical classes using pie charts, one compatible with less processed material and the other reflecting a different formation site or possible evolution of the nucleus material with time.

We demonstrated that the quotients of different MRs can help in developing a chemical classification, since they can reveal trends and similarities among comets not visible when comparing absolute values. In this way, we developed an

Table 7
K and M Factors for the Studied Comets

Comet	K[a]	M[a]	Group[b]
C/2007 N3	0.88	2.34	1
C/1999 S4	0.05*	0.18*	1, 2[c]
C/1999 H1	1.78	2.63	1
C/2009 P1	0.19	0.45	2
C/2012 S1	0.54*	0.43*	2
C/2012 F6	0.17	0.77	2
C/1999 T1	0.10	0.71	2
C/2000 WM_1	2.21	1.44	2, 3[c]
C/2013 R1	0.20	0.66	2
C/2001 A2	2.04	0.88	3
C/2004 Q2	0.20	0.72	2, 3[c]
C/2007 W1	2.67	1.91	3
8P	3.71*	2.63*	3[c]
103P	8.10*	7.21*	3[c]
73PB	0.95*	0.64*	2, 3[c]
73PC	0.70*	1.06*	2, 3[c]
17P	N.A.	N.A.	N.A.
10P	N.A.	N.A.	N.A.
9P	0.45*	1.56*	1, 2[c]
2P	2.12*	1.67*	3[c]

Notes.
[a] An asterisk indicates that the value was retrieved using at least one upper limit.
[b] Groups are numbered following the description in Section 3.2.2.
[c] Tentative classification.

alternative classification, still compatible with the pie chart approach, and somehow correlated to the orbital parameters of the analyzed comets. This method allowed us to compare our results with recent protoplanetary disk models, considering, for example, the interrelationship between $MR(CH_3OH)/MR(CO)$ and $MR(C_2H_6)/MR(CH_4)$. We defined two factors, K and M, that can be associated with increased processing of the cometary material in time and/or an increasing formation distance of a comet (for long-period comets). For short-period comets, we associate an evolution of the most volatile species while in their current inner solar system orbits. It is very important to underline that our studies are based on a still-limited sample, giving a quite simplified view of the formation of comets. In this respect, it is still not possible to unequivocally trace back the origins of the selected targets or to produce a firm taxonomical classification for these bodies. However, increasing the statistical sample may offer the possibility of investigating the origins and evolution of the cometary material using this approach and perspective.

In the near future, we aim to complete our revisions of the spectra in our archive, which comprises high-resolution IR spectroscopic observations of comets since 1995. More than half of the collected data still need to be revisited or even analyzed for the first time. In theory, there is the possibility of creating a complete and consistent sample of more than 60 comets that will constitute a much better cross section. In addition, the reanalysis of many data sets may also help by addressing some of the 2σ upper limits, further improving our statistics. We are also revising and exploring other parameters, such as isotopic and ortho-to-para ratios, and testing their cosmogonic origins; correlating these updated values to the relationships that we presented here will allow a more comprehensive view of the nature of comets. Finally, a comparison with results obtained from observations at different wavelengths may reveal interesting aspects of the chemistry in the coma. We plan to report these additional studies in three or more separate forthcoming manuscripts.

These investigations are expected to provide a new metric of comparisons between cometary composition and protoplanetary disk models, improving our understanding of the formative origin of these bodies.

We thank the reviewers Neil Dello Russo and Jacques Crovisier for helpful comments that greatly improved the manuscript. This work was supported by the NASA Astrobiology Institute (13-13NAI7-0032 to Goddard Space Flight Center; PI: M. J. Mumma) and the NASA Emerging Worlds Program (EW15-57 to Goddard Space Flight Center; PI: G. L. Villanueva). This research has made use of the Keck Observatory Archive (KOA), which is operated by the W. M. Keck Observatory and the NASA Exoplanet Science Institute (NExScI) under contract with the National Aeronautics and Space Administration. The authors wish to recognize and acknowledge the very significant cultural role and reverence that the summit of Maunakea has always had within the indigenous Hawaiian community. We are most fortunate to have the opportunity to conduct observations from this mountain.

Appendix A
Comet-by-comet Results and Comparisons[8]

Hereafter, we shortly introduce the observing time and conditions for each comet (except for the ones described in Lippi et al. 2020), and we provide a comparison of our results with previously reported ones, together with a short discussion of the factors that may have contributed to the observed differences. Our retrieved rotational temperatures, nucleus centered production rates, grow factors, global production rates and mixing ratios are provided as online tables, with Table A1 shown as an example.

A1. C/2007 N3 (Lulin)

Comet C/2007 N3 (Lulin) was discovered on 2007 July 11 (Young 2007), and it was classified as a dynamically new comet from the OC family probably at its first apparition in the inner solar system. It reached perihelion (1.21 au) on 2009 January 10 and its closest approach to Earth (0.41 au) on 2009 February 24. From our archive, we selected the 2009 January 31 observations for the KL2 setting and 2009 February 1 observations for the KL1 and MW settings. We compared our results (see Table A1) with the corresponding values reported in Table 5 of Gibb et al. (2012). Their analysis partially uses the same models we adopted, so we do not expect important changes in the results. In fact, we measure the following.

1. Similar rotational temperatures for water: (65 ± 1) and (68 ± 4) K versus (67 ± 2) and (69 ± 1) K; lower but still comparable temperatures for CH_3OH and HCN, (57 ± 3) versus $(67\ +7/-6)$ K and (65 ± 10) versus (72 ± 6) K, respectively; and a lower temperature for CH_4, $(59\ +4/-5)$ K versus (68 ± 2) K. For C_2H_6, we measure a rotational temperature of $(77\ +13/-10)$ K from setting KL1, comparable with the one of (74 ± 8) K previously

[8] For comets C/1999 S4 (LINEAR), C/2001 A2 (LINEAR), C/2007 W1 (Boattini), C/2012 S1 (ISON), and C/2012 F6 (Lemmon), see Lippi et al. (2020).

Table A1
Rotational Temperatures, Production Rates, and MRs for C/2007 N3[a]

Date	Setting	Molecule	T_{rot}[b] (K)	Q_{nc}[c] ($\times 10^{26}$ mol s^{-1})	GF	Q_{tot} ($\times 10^{26}$ mol s^{-1})	MRs (% w.r.t. H_2O)
31-Jan-2009	KL2	H_2CO	(68)	0.81 ± 0.13	1.64 ± 0.06	1.33 ± 0.21	0.15 ± 0.02
		CH_4	59 +4/−5	7.20 ± 0.26		11.8 ± 0.6	1.29 ± 0.06
		HCN	67 +7/−6	0.77 ± 0.07		1.27 ± 0.12	0.14 ± 0.01
		C_2H_2	(68)	0.46 ± 0.09		0.76 ± 0.15	0.08 ± 0.02
		NH_3	(68)	<1.54		<2.53	<0.28
		H_2O	68 ± 4	556 ± 19		912 ± 46	100
1-Feb-2009	KL1	CH_3OH	57 ± 3	34.59 ± 1.18	1.48 ± 0.01	51.2 ± 1.78	3.82 ± 0.15
		C_2H_6	77 +13/−10	7.20 ± 0.30		10.7 ± 0.44	0.80 ± 0.04
		H_2O	65 ± 1	906 ± 16		1340 ± 25	100
		NH_3	(65)	2.44 ± 1.41		3.62 ± 2.06	0.27 ± 0.16
	MW	H_2O	63 ± 2	1427 ± 27	1.64 ± 0.11	2340 ± 163	100
		CO	77 ± 11	37.8 ± 2.0		62.3 ± 5.3	2.66 ± 0.15

Notes.
[a] Data for all other comets are available in machine-readable format.
[b] Values in parentheses are assumed.
[c] Calculated for a common rotational temperature of 68 K for January 31, 65 K for the February 1 KL1 setting, and 63 K for the February 1 MW setting.
(This table is available in its entirety in FITS format.)

measured from KL2. We added an estimate for the rotational temperature of CO (77 ± 11) K.

2. Lower values for the total water production rate: between about −15% and −30%, $(912 \pm 46) \times 10^{26}$ versus $(1351 \pm 84) \times 10^{26}$ mol s^{-1} (KL2-31 2009 January) and $(1340 \pm 25) \times 10^{26}$ versus $(1565 \pm 48) \times 10^{26}$ mol s^{-1} (KL1-1 2009 February), except for the MW setting, where we measure a higher value $(2340 \pm 163) \times 10^{26}$ versus $(2013 \pm 50) \times 10^{26}$ mol s^{-1} (+16%).
3. Comparable MRs for CH_3OH (3.82 ± 0.15 versus 3.62 ± 0.18, +5.5%), HCN (0.14 ± 0.01 versus 0.124 ± 0.009, +12.9%), C_2H_6 (0.80 ± 0.04 versus 0.86 ± 0.04, −7.0%), C_2H_2 (0.08 ± 0.02 versus 0.066 ± 0.011, +21.2%), and CH_4 (1.30 ± 0.07 versus 1.19 ± 0.06, +9.2%) and higher values for H_2CO (0.15 ± 0.02 versus 0.11 ± 0.02, +36.4%) and CO (2.66 ± 0.15 versus 2.17 ± 0.11, +22.6%); the measure we have for NH_3 on 2009 January 31 KL2 is comparable with the previous measure obtained using the same setting but on 2009 February 1 (0.27 ± 0.16 versus 0.28 ± 0.06, −3.6%).

We attribute some of the dissimilarities to issues with the removal of residual fluxes in the sky-subtraction process and the calculation of offsets in the faint cometary signatures. This is particularly notable for H_2CO with very weak lines, in which small offsets could lead to substantial differences. Furthermore, we employed different telluric models, now parameterized with NASA/MERRA-2 climatology and synthesized with PSG. Other smaller differences are probably due to intrinsic uncertainties related to the noise of the astronomical observations and slight human interaction in the data analysis.

A2. C/1999 H1 (Lee)

Comet C/1999 H1 (Lee) is a long-period comet from the OCs discovered in 1999 February. We reduced the data relative to 1999 August 19 and 20 and compared the results with Mumma et al. (2001b), who first published a compositional survey for this comet, and Dello Russo et al. (2006), who reanalyzed the data using a then-updated water fluorescence model (Dello Russo et al. 2005). Our data differ in many aspects from the previous ones, particularly in the following.

1. We measure a rotational temperature for water of (70 ± 2) K, while Mumma et al. (2001b) assumed a temperature of 75 K and Dello Russo et al. (2006) measured (76 +4/−3) K. We measure a lower temperature for C_2H_6 and HCN: (68 +7/−6) versus (80 +25/−19) K and (61 +11/−8) versus (72 ± 8) K, respectively. We do not retrieve a T_{rot} for CO, but we add an estimate for CH_3OH, slightly lower with respect to other molecules of (59 ± 3) K.
2. The updated water production rates are comparable within the error bars with the previous ones.
3. For CH_3OH, we measure an MR much higher than the previously reported one (+52% with respect to Mumma et al. 2001b and +100% with respect to Dello Russo et al. 2006), as well as for C_2H_6 (+33% with respect to Mumma et al. 2001b and +25% with respect to Dello Russo et al. 2006). Our measure of HCN is instead lower than the one presented in Mumma et al. (2001b; −17%) but comparable with the one revisited in Dello Russo et al. (2006). We see an important decrease in C_2H_2 (about −65% with respect to both of the previous results). The CO is comparable within the error bars with the result in Mumma et al. (2001b; 1.48 ± 0.37 versus 1.8 ± 0.8, −18%). Finally, we report for the first time a measure for NH_3 and H_2CO.

Comet C/1999 H1 is among the first comets observed with NIRSPEC, and it was analyzed when many quantum molecular models were still lacking and empirical *g*-factors were used to interpret the identified molecular emission lines. In addition, Mumma et al. (2001b) calculated the atmospheric transmittance using the spectrum synthesis program (SSP; Kunde & Maguire 1974) with a priori atmospheric profiles and accessing the HITRAN-1992 molecular database (Rothman et al. 1992). For this reason, both the use of new quantum molecular models and PUMAS/PSG have played an important role in the many differences that we observe between our values and the previously reported ones.

A3. C/2009 P1 (Garradd)

Comet C/2009 P1 (Garradd) was discovered on UT 2009 August 13 and classified as a nearly isotropic (long-period) comet from the OC reservoir. We analyzed archival data relative to three nights (2011 October 13, preperihelion, and 2012 January 9 and 10, postperihelion). Results relative to this comet were presented in DiSanti et al. (2014), who reported the results relative to 2011 October 13 and 2012 January 8. Considering that the comet was analyzed more recently, we do not expect strong discrepancies between our and the previous work.

1. From the analysis of the October 13 observations, we got comparable rotational temperatures for H_2O, (50 ± 2) versus the assumed (48 ± 4) K, and for C_2H_6, $(46\ +8/-6)$ versus $(44\ +9/-7)$ K. We find a higher but still comparable temperature for CH_3OH, $(52\ +5/-4)$ versus $(45\ +6/-5)$ K, but a much higher temperature for HCN, $(71\ +10/-8)$ versus $(55\ +6/-7)$ K. We do not report a value of T_{rot} for CH_4 and CO. For 2012 January 9 and 10, we measure rotational temperatures for H_2O, C_2H_6, CH_3OH, and HCN that are comparable with the one relative to water reported by DiSanti et al. (2014).
2. On average, we got lower water production rates that are still comparable within the 1σ error bars with the previous ones.
3. We retrieve similar values for CH_3OH (+7%), HCN (+9%), C_2H_6 (+5%), and CO (−15%) and a marginally higher value for CH_4, (1.02 ± 0.07) versus (0.84 ± 0.08) (+21%). Our values for NH_3 and C_2H_2 are much higher than the previous ones: (1.03 ± 0.81) versus (0.50 ± 0.16) (+106%) and (0.16 ± 0.04) versus (0.06 ± 0.02) (+167%). Our upper limit for H_2CO is instead lower with respect to the previous detection (<0.05 versus 0.11 ± 0.04).

The major observed differences are possibly introduced through intrinsic uncertainties related to the noise of the astronomical observations and slight human interaction in the data analysis. In addition, DiSanti et al. (2014) modeled the atmosphere using the line-by-line radiative transfer model by Clough et al. (2005), while we employed PUMAS/PSG; the use of different atmospheric transmittance models may have impacted the results from those settings where the atmospheric water lines can have a strong influence (e.g., at about 3.3 μm, that is, the region where NH_3 and C_2H_2 are usually detected). Finally, we are comparing different observing dates in 2012 January, and although they are close in time, we cannot exclude possible variations in molecular production rates related to the activity of the comet.

A4. C/1999 T1 (McNaught–Hartley)

Comet C/1999 T1 (McNaught–Hartley) is a dynamically young long-period comet discovered on 1999 October 7. Among our sample, it is the comet that was less analyzed in the past. We compared our results with the little information relative to the January 14 observations reported in Mumma et al. (2001a), Gibb et al. (2003), and Mumma et al. (2003). We found many important differences with respect to the previous analyses.

1. For 2001 January 14, we found a lower rotational temperature for water: (60 ± 4) versus 70 K assumed in the previous analysis. Our water rotational temperature is comparable with the newly retrieved temperatures for CH_3OH and C_2H_6: $(57\ +4/-3)$ and $(65\ +13/-9)$ K, respectively. In February, we got slightly lower rotational temperatures for the same molecules, $(52\ +7/-8)$ K for H_2O, (49 ± 3) K for CH_3OH, and (41 ± 5) K for C_2H_6, and we added an estimate for HCN: $(52\ +7/-8)$ K.
2. Our water production rate measured on January 14 is comparable with the preliminary value reported in Gibb et al. (2003), $(654 \pm 100) \times 10^{26}$ versus $(570 \pm 24) \times 10^{26}$ mol s^{-1}, but much lower than the one reported in Mumma et al. (2003; 1600×10^{26} mol s^{-1}), the latter derived from the OH^* prompt emission analysis.
3. Our retrieved MRs for CH_3OH, CH_4, and C_2H_6 are all much higher than the previous ones (about +115%, +94%, and +60%, respectively), while we measure lower values for HCN ((0.15 ± 0.03) versus (0.37 ± 0.08)) and CO ((13.5 ± 2.6) versus (17 ± 5)). We completed the molecular inventory for this comet, adding a measure for C_2H_2 and H_2CO ((0.28 ± 0.07) and (0.14 ± 0.05), respectively) and an upper limit for NH_3 (<1.1).

Comet C/1999 T1 is among the first comets that were observed using IR high-resolution spectroscopy, and its data were analyzed far before 2011, so the combination of more complete quantum molecular models and updated atmospheric transmittance models and reduction tools has contributed in large amount to the differences that we observe. For example, as we noticed for comet C/1999 S4 in Lippi et al. (2020), the higher value of HCN measured in the past could originate from previously unrecognized blended water lines in the same spectral region, which translated into a previous overestimation of the HCN production rate.

A5. C/2000 WM_1 (LINEAR)

The OC comet C/2000 WM_1 is a dynamically young long-period comet with perihelion (0.555 au) on 2002 January 22; it made its closest approach to Earth (0.316 au) on 2001 December 2. Despite this comet being observed in 2001, the corresponding data reduction is more recent (Radeva et al. 2010). We find the following differences and similarities.

1. For November 23, our rotational temperature derived from H_2O is comparable with the one previously reported: (70 ± 3) versus (70 ± 1) K. The one retrieved for HCN is lower but still comparable within the errors: $(69\ +8/-6)$ versus $(76\ +17/-13)$ K. For November 24, we retrieve a higher water temperature, (78 ± 5) K. For both of the observing nights, we added the measure of the rotational temperatures for CH_3OH and C_2H_6.
2. Our water production rates are systematically higher than the ones reported in Radeva et al. (2010), about $(340 \pm 19) \times 10^{26}$ versus $(209 \pm 17) \times 10^{26}$ mol s^{-1} and $(294 \pm 14) \times 10^{26}$ versus $(238 \pm 31) \times 10^{26}$ mol s^{-1}, and particularly high if we consider the MW setting: about $(494 \pm 54) \times 10^{26}$ versus $(210 \pm 29) \times 10^{26}$ mol s^{-1}.
3. We retrieve MRs comparable within 1σ uncertainties for CH_3OH, C_2H_6, and CO. We instead find higher values for HCN and CH_4: (0.21 ± 0.01) versus (0.15 ± 0.01), +40% and (0.41 ± 0.03) versus (0.34 ± 0.03), +21%, respectively. Our value for H_2CO is much lower than the previous one: (0.06 ± 0.02) versus (0.20 ± 0.03), −70%, while our measure of C_2H_2 (0.06 ± 0.02) is higher than

the upper limit previously reported. We completed the molecular inventory for this comet, adding a 2σ upper limit for NH_3 (<0.42).

The differences we observe are mainly referable to different quantum molecular models used in the analysis; for example, for methanol and formaldehyde, Radeva et al. (2010) reported the analysis of the individual Q branch only, while for both species, we adopted the respective full rovibrational band. Other small differences may have been introduced through the adoption of different atmospheric models (GENLN2 spectral synthesis program, Edwards 1992, versus PUMAS/PSG) and analysis approaches.

A6. C/2013 R1 (Lovejoy)

Comet C/2013 R1 was discovered on 2013 September 7; its orbital parameters identify it as a nearly isotropic (long-period) comet originating from the OC. Even if the spectra of this comet were reduced and analyzed using more recent algorithms by Paganini et al. (2014), we can find some differences in the results.

1. The rotational temperatures that we retrieved are in general systematically higher (a maximum difference of about +20% for water on October 22) but still comparable within the uncertainties with the previously reported ones.
2. Our water production rates for October 22, 24, and 27 and November 7 are also systematically higher but comparable within the 2σ error bars with the previous ones. For the October 25 and 29 observations, we retrieve particularly higher values: $(400 \pm 37) \times 10^{26}$ versus $(232 \pm 33) \times 10^{26}$ mol s^{-1} and $(299 \pm 32) \times 10^{26}$ versus $(145 \pm 40) \times 10^{26}$ mol s^{-1}, respectively.
3. If we consider the weighted averages along all of the observing nights, our MRs are comparable within the 1σ error bars with the previous ones. Our value for CH_4 is slightly higher than the previous one ((1.17 ± 0.04) versus (0.89 ± 0.06), +32%), while the NH_3 measure is much higher (+1380%). For H_2CO and C_2H_2, we managed to retrieve measures that are higher than the previously reported upper limits.

We can assume that the small observed differences in rotational temperatures, water production rates, and MRs of CH_3OH, C_2H_6, HCN, and CH_4 depend mainly on the noise fluctuations in the spectra and slight human interaction in the data analysis, plus some dependence on the telluric atmospheric models.

A7. C/2004 Q2 (Machholz)

Comet C/2004 Q2 (Machholz) was discovered on 2004 August 27, and it is classified as a long-period comet whose origin is most likely the OC. The comet passed perihelion on 2005 January 24 and had its closest approach to Earth at 0.35 au on 2005 January 6. Here we present data relative to 2004 November 28 and 2005 January 19, and we compare our results with the one reported in Bonev et al. (2009). We find the following differences.

1. For water, we obtain the same rotational temperature for the first observing night (about 85 K) but a lower one for the second observing night ((80 ± 2) versus (93 ± 2) K). For HCN instead, we have higher temperatures for both the observing nights: $(94\ +6/-5)$ versus (76 ± 9) K and $(89\ +5/-4)$ versus (76 ± 2) K. We do not have an estimate for the rotational temperature of CO, but we measured the ones of C_2H_6: $(91\ +16/-12)$ and $(90\ +12/-10)$ K for the first and second observing nights, respectively. Our rotational temperature of methanol is lower with respect to the other species: $(61\ +3/-4)$ and $(71\ +2/-1)$ K for the first and second observing nights, respectively.
2. On 2004 November 28, we retrieve water production rates that are much lower than the ones reported in Bonev et al. (2009; about −45%). On 2005 January 19, our values are comparable with the previous ones.
3. Our MRs are systematically lower with respect to the previous ones: CH_3OH, −15%; NH_3, −35%; H_2CO, −44%; C_2H_2, −24%; CH_4, −10%; and CO, −5%. The exceptions are HCN, for which we measure a value similar to the previously reported one, and C_2H_6, which instead shows an increment of +23%.

Since the comet was observed and analyzed before 2011, the differences we observe are mainly related to the combination of the use of different models for the interpretation of the spectra and the synthesis of the atmosphere. For example, Villanueva et al. (2012), using the latest CH_3OH model, reported an MR of $(42.0 \pm 2.0) \times 10^{26}$ mol s^{-1} measured on January 19 that is the same as the value that we measure, $(42.6 \pm 1.0) \times 10^{26}$ mol s^{-1}. The corresponding MR of (1.54 ± 0.07) in Villanueva et al. (2012), retrieved using the water production rate from Bonev et al. (2009), would correspond to a comparable MR for CH_3OH (1.74 ± 0.08) if using our production rate for water.

A8. 8P/Tuttle

Comet 8P/Tuttle is dynamically classified as a Halley-type comet, and it was observed extensively during its favorable apparition in 2007/2008. We found some differences with respect to Bonev et al. (2008), who reported rotational temperatures, production rates, and MRs obtained from the analysis of the same NIRSPEC data sets.

1. For water in KL1, we obtain a lower rotational temperature, (50 ± 2) versus (60 ± 15) K; our value is comparable with the one measured for the KL2 setting. Our measured $T_{\rm rot}$ for HCN is also lower than the previous one (on average, about 42 versus 51 K). In addition, we report rotational temperatures for CH_3OH and C_2H_6 of (42 +2/-1) and (51 +18/-10) K, respectively.
2. Our water production rates are about −10% lower on average but still comparable within the uncertainties with the ones reported in Bonev et al. (2008).
3. Our MRs for methanol and ethane are higher than the previously reported ones: CH_3OH, (2.61 ± 0.13) versus (2.18 ± 0.07), +20%, and C_2H_6, (0.30 ± 0.03) versus (0.24 ± 0.03), +25%. Our measure of HCN is much higher than the previous one, (0.16 ± 0.02) versus (0.07 ± 0.01), +129%, while the one relative to methane is lower, (0.25 ± 0.02) versus (0.37 ± 0.07), −32%. If we consider the upper limits, we have a comparable value for C_2H_2 (<0.04 versus <0.03) and a higher one for CO (<0.84 versus <0.25). We added a measure for H_2CO

(0.10 ± 0.02 versus <0.02) and one for NH_3 (0.72 ± 0.38), not reported in previous works.

Being analyzed before 2011, we expected some of the observed differences that we associate mainly with the employed quantum fluorescence models for the interpretation of the emission lines in the spectra and the different atmospheric transmittance model. The case of HCN is interesting, since past papers reported a depletion of this molecule in 8P (Kobayashi et al. 2010; Bonev et al. 2008; Böhnhardt et al. 2008), while our retrieved value is closer to the median value that we measure in comets for this molecule and compatible with the abundance of CN that was observed in the optical during the 2007/2008 apparition.

A9. 103P/Hartley 2

We compared our results for 103P with the ones reported in Dello Russo et al. (2011), Mumma et al. (2011), and Kawakita et al. (2013).

1. Our rotational temperatures for October 17 and 21 are comparable with the ones presented in Kawakita et al. (2013), as well as the ones measured by Mumma et al. (2011) on October 19 and 22. Using the November 4 data, we obtain similar-to-lower rotational temperatures with respect to Dello Russo et al. (2011), except for C_2H_6, for which we measure a much higher temperature ($84\ +11/-9$ versus $63\ +8/-7$).
2. Our production rates for water are comparable within the uncertainties with the previously reported ones in Kawakita et al. (2013) and Mumma et al. (2011) for the October measurements and Dello Russo et al. (2011) for the November data.
3. Considering the averaged MRs, the value we measured for CH_3OH is higher than the previously reported one (+45%); we also retrieved higher values for C_2H_6 and HCN, even if to a lesser extent (+14.5% and +10.2%, respectively). We measured lower values for NH_3 and H_2CO (−26.4% and −33.3%, respectively). Our weighted average for C_2H_2 is comparable with the one retrieved from the combination of previously reported data.

The differences that we observe are most likely related to diverse fluorescence models that the different groups applied to the spectra combined with the different atmospheric models employed to synthesize the spectral transmittance.

A10. 73P/Schwassmann–Wachmann

Comet 73P/Schwassmann–Wachmann is a JF comet that probably originated in the KB. During its 1995 apparition, the comet split into many fragments, increasing the overall gas production rate by more than an order of magnitude from the previous apparition. We compared our results with the ones reported in Dello Russo et al. (2007).

1. For both fragments, we obtain similar rotational temperatures for H_2O, HCN, and C_2H_6. Moreover, we give an estimate for the rotational temperature of CH_3OH that is slightly lower than the ones relative to the other species (e.g., on May 14, we measure a T_{rot} of $(70\ +8/-7)$ K for CH_3OH and (92 ± 10) K for H_2O).
2. For fragment B, we find different water production rates with respect to earlier results: $(73 \pm 4) \times 10^{26}$ versus $(121 \pm 9) \times 10^{26}$ mol s^{-1} and $(112 \pm 54) \times 10^{26}$ versus $(50 \pm 29) \times 10^{26}$ mol s^{-1} on May 14 and $(52 \pm 3) \times 10^{26}$ versus $(121 \pm 8) \times 10^{26}$ mol s^{-1} on May 15. For fragment C, we measure water production rates that are always lower than the previously reported ones (on average, about −20%).
3. We measure higher MRs for methanol (+105% and +147% for fragments B and C, respectively) and slightly higher values for C_2H_6 (+13% and +20% for fragments B and C, respectively) and HCN in fragment C (+35%). For C_2H_2, we measure contrasting values (about +15% and −42% for fragments B and C, respectively). For H_2CO, we find values that are about −80% (fragment B) and −54% (fragment C) lower than the ones reported in Dello Russo et al. (2007).

As for other comets whose data were analyzed before 2011, we can trace back the dissimilarities to the different models used for the interpretation of the fluorescence emissions and different atmospheric transmittance models employed in the reduction. For example, the C_2H_6 production rates were previously determined following Dello Russo et al. (2001), while we used the more recent model from Villanueva et al. (2011b). In addition, Dello Russo et al. (2007) reproduced the observed atmosphere using the SSP (Kunde & Maguire 1974), which accessed the HITRAN-1992 molecular database (Rothman et al. 1992).

A11. 17P/Holmes

Comet 17P/Holmes is a JF comet that probably originated in the KB and experienced an extraordinary outburst on 2007 October 24. When we compare our results with the corresponding ones reported in Dello Russo et al. (2008), we can see some differences and similarities.

1. On October 27, for H_2O and HCN, we measure rotational temperatures similar to those previously reported. On October 30, we find a similar temperature for HCN, but we measure a water rotational temperature of (70 ± 3) K, slightly higher than the one of 60 K assumed by Dello Russo et al. (2008). We do not report the rotational temperature for C_2H_6, but instead we manage to measure the one relative to methanol $(70\ +7/-6)$ K that is comparable with the one we measure for water.
2. Our water production rate measured on October 27 is lower than the one in Dello Russo et al. (2008): $(3650 \pm 233) \times 10^{26}$ versus $(4500 \pm 570) \times 10^{26}$ mol s^{-1}. We instead measure a water production rate similar to the previous one on October 30.
3. Our methanol abundance is much higher than the previous one, (4.30 ± 0.43) versus (2.37 ± 0.40), +81%, as well as the C_2H_6 one, (2.31 ± 0.14) versus (1.80 ± 0.23), +28%. The HCN MRs are instead similar within the uncertainties (+13.0%). Compared to Dello Russo et al. (2008), we measure a lower abundance of acetylene but still comparable within the error bars: (0.24 ± 0.11) versus (0.34 ± 0.05), −29%. Finally, we introduce for the first time a measure for NH_3 and a 2σ upper limit estimate for H_2CO.

The dissimilarities from previous results are probably due to the different models applied to retrieve the production rates; for example, Dello Russo et al. (2008) followed Dello Russo et al. (2005) for H_2O, Magee-Sauer et al. (1999) for HCN, Brooke et al. (1996) for C_2H_2, and Dello Russo et al. (2001) for C_2H_6. The different models used to describe the atmospheric transmittance (FASCOD3 transmittance model, accessing the HITRAN-2004 Molecular Data Base (Rothman et al. 2005), versus PUMAS/PSG) may have also contributed to these differences.

A12. 10P/Tempel 2

Comet 10P/Tempel 2 was discovered by Ernst Wilhelm Liebrecht Tempel in 1873, and it is classified as an ecliptic comet belonging to the Jupiter dynamical family. With respect to Paganini et al. (2012), we measure the following:

1. The same rotational temperature for H_2O. While Paganini et al. (2012) reported an HCN rotational temperature of $(36\ +13/-9)$ K, we did not manage to retrieve a sufficiently sensitive value. On the other hand, we measure $(27\ +3/-4)$ K for CH_3OH and $(24\ +9/-12)$ K for C_2H_6.
2. Our water production rate is about 30% lower than the previous one: $(129 \pm 10) \times 10^{26}$ versus $(184 \pm 12) \times 10^{26}$ mol s^{-1}.
3. For all species, we measure MR values that are comparable within the 1σ uncertainties with the ones previously presented in Paganini et al. (2012), with NH_3 presenting the highest relative difference (+34.9%).

Comet 10P/Tempel 2 was partially analyzed using our same models, so there are only minor differences between our results and the previous ones, possibly related to different human influences in the data analysis and fluctuations in the noise level.

A13. 9P/Tempel 1

The JF comet 9P/Tempel 1 was the target of the NASA Deep Impact mission, and there was an important observing campaign before, during, and after the impact event. Here we report the results obtained from observations pre- (2005 July 3 and 4, KL1) and postimpact (2005 July 4 and 5, KL1, KL2, and MW), and we compare the results with the corresponding ones previously presented in Mumma et al. (2005).

1. On June 3, our rotational temperature retrieved for water is comparable with the one previously reported for HCN: (27 ± 3) versus $(33\ +8/-6)$ K. For July 4 and 5, it is comparable with the one reported in Mumma et al. (2005; about (35 ± 4) versus (38 ± 6) K for the first night and (52 ± 14) versus 40 K (assumed) for the second night). In addition, for the postimpact data, we measure rotational temperatures for CH_3OH of (32 ± 8) K and C_2H_6 of (37 ± 3) K, both comparable with our estimate for water.
2. We find a lower water production rate preimpact $((61 \pm 19) \times 10^{26}$ versus $(104 \pm 17) \times 10^{26}$ mol s^{-1}) and a higher one right after the impact $((148 \pm 11) \times 10^{26}$ versus $(98 \pm 3) \times 10^{26}$ mol s^{-1}). For July 5, we find a very low water production rate in comparison to the previously reported one: $(83 \pm 23) \times 10^{26}$ versus $(200 \pm 40) \times 10^{26}$ mol s^{-1}.
3. If we compare the final MRs calculated as the weighted average along the three observing dates, we find that our MRs for CH_3OH, HCN, C_2H_6, and CH_4 are higher than the previous ones (+98.2%, +20%, +24%, and +22%, respectively), while H_2CO is much lower (0.18 ± 0.07 versus 0.84 ± 0.18, −79%). We find upper limits for C_2H_2 and CO, in contrast with the detections reported in Mumma et al. (2005). We introduced for the first time a measure for NH_3 (1.14 ± 0.72).

Comet 9P was analyzed well before 2011, and as assessed for other comets in this list, the use of updated quantum molecular models combined with improved atmospheric transmittance models contributed in large part to the differences that we observe.

A14. 2P/Encke

Comet 2P/Encke is an ecliptic comet with $T_J = 3.025$, a period of 3.3 yr, and an aphelion distance of 4.09 au; it was observed on 2003 November 4–6 during its close approach to the Earth. We compared our results with the one presented in Radeva et al. (2013), which analyzed the comet using most of the same tools we used. With respect to their previous findings, we measure the following.

1. About the same rotational temperatures occur for H_2O and HCN, and, for November 5, there is a higher (but still comparable) rotational temperature value for CH_3OH: (30 ± 2) versus $(24\ +6/-5)$ K.
2. The water production rates are equivalent within a 1σ uncertainty to the previous ones, but not for November 6, when we measure a slightly higher value (about $(37 \pm 3) \times 10^{26}$ versus $(26 \pm 2) \times 10^{26}$ mol s^{-1}).
3. The molecular MRs are comparable within a 1σ error bar with the previously presented ones, except for C_2H_6, which in our case is +74.2% higher. Our 2σ upper limits are comparable to the previous ones, except for CO, for which we measure a higher value. We introduced for the first time a 2σ upper limit for NH_3.

As expected, our values are mainly consistent with the previous ones, except for some small differences that can be explained by fluctuations in the noise level.

Appendix B
Spearman Correlation Factors and Statistics

The Spearman rank correlation coefficient ρ_{Sp} measures how well the relationship between two variables can be described using a monotonic function, not necessarily linear. Compared to the Pearson correlation, the Spearman correlation uses ranks and does not assume that the variables are normally distributed. This type of analysis can therefore be used in many cases in which the assumptions of the Pearson correlation (continuous-level variables, linearity, and normality) are not met.

For the Spearman correlation values reported in this paper, we used the IDL function "*r_correlate*," based on the book "Numerical Recipes: The Art of Scientific Computing" (Second Edition, Cambridge University Press, 2007). For a sample of size n, the variables are converted to ranks (x_i, y_i),

and $\rho_{\rm Sp}$ is computed as

$$\rho_{\rm Sp} = \frac{\sum_i (x_i - \bar{x})(y_i - \bar{y})}{\sqrt{\sum_i (x_i - \bar{x})^2 \sum_i (y_i - \bar{y})^2}}.$$

If there are no tied ranks in the data, the previous equation can be approximated to

$$\rho_{\rm Sp} = 1 - \frac{6\sum D^2}{n(n^2 - 1)},$$

where $D = (x_i - y_i)$ denotes the difference (distance) between the two ranks for each observation, and n is the number of measures.

For reasonable sample sizes of $n \geqslant 30$, the statistical significance uses the t-distribution:

$$t = \frac{\rho_{\rm Sp}\sqrt{n-2}}{\sqrt{1 - {\rho_{\rm Sp}}^2}}.$$

The p-values are then retrieved by interpolating the t-test value to the corresponding incomplete beta function integral computed for the equivalent degrees of freedom.

The test of significance used in this procedure indicates that for $p < 0.05$, there is a probability of more than 95% that the null hypothesis is verified, i.e., that the observed correlation is not caused by random effects. However, the resulting statistic becomes inaccurate for smaller sample sizes ($n < 30$), and the test should be used with caution. In fact, the t-distribution shape depends on the degrees of freedom, showing shorter and thicker tails as the size of the sample decreases. This will translate into increased t-values and, consequently, into small p-values, suggesting that a correlation may be significant even when it is not.

ORCID iDs

M. Lippi https://orcid.org/0000-0001-9185-878X
G. L. Villanueva https://orcid.org/0000-0002-2662-5776
M. J. Mumma https://orcid.org/0000-0003-4627-750X
S. Faggi https://orcid.org/0000-0003-0194-5615

References

A'Hearn, M. F., Millis, R. C., Schleicher, D. O., Osip, D. J., & Birch, P. V. 1995, Icar, 118, 223
Aikawa, Y., Umebayashi, T., Nakano, T., & Miyama, S. M. 1999, ApJ, 519, 705
Altwegg, K., Balsiger, H., Hänni, N., et al. 2020, NatAs, 4, 533
Bergin, E. A., & Cleeves, L. I. 2018, Handbook of Exoplanets (Berlin: Springer), 137
Bockelée-Morvan, D., & Biver, N. 2017, RSPTA, 375, 20160252
Böhnhardt, H., Mumma, M. J., Villanueva, G. L., et al. 2008, ApJL, 683, L71
Bonev, B. P. 2005, PhD thesis, The University of Toledo
Bonev, B. P., Dello Russo, N., DiSanti, M. A., et al. 2020, BAAS, 52, 316.02
Bonev, B. P., Mumma, M. J., DiSanti, M. A., et al. 2006, ApJ, 653, 774
Bonev, B. P., Mumma, M. J., Gibb, E. L., et al. 2009, ApJ, 699, 1563
Bonev, B. P., Mumma, M. J., Radeva, Y. L., et al. 2008, ApJL, 680, L61
Bonev, B. P., Villanueva, G. L., DiSanti, M. A., et al. 2017, AJ, 153, 241
Bosman, A. D., Walsh, C., & van Dishoeck, E. F. 2018, A&A, 618, A182
Brooke, T. Y., Tokunaga, A. T., Weaver, H. A., et al. 1996, Natur, 383, 606
Clough, S. A., Shephard, M. W., Mlawer, E. J., et al. 2005, JQSRT, 91, 233
Cochran, A. L., Barker, E. S., & Gray, C. L. 2012, Icar, 218, 144
Cochran, A. L., Levasseur-Regourd, A.-C., Cordiner, M., et al. 2015, SSRv, 197, 9
Cottin, H., & Fray, N. 2008, SSRv, 138, 179
Dello Russo, N., Bonev, B. P., DiSanti, M. A., et al. 2005, ApJ, 621, 537
Dello Russo, N., DiSanti, M. A., Mumma, M. J., Magee-Sauer, K., & Rettig, T. W. 1998, Icar, 135, 377
Dello Russo, N., Kawakita, H., Vervack, R. J., & Weaver, H. A. 2016, Icar, 278, 301
Dello Russo, N., Mumma, M. J., DiSanti, M. A., et al. 2006, Icar, 184, 255
Dello Russo, N., Mumma, M. J., DiSanti, M. A., Magee-Sauer, K., & Novak, R. 2001, Icar, 153, 162
Dello Russo, N., Vervack, R. J., Weaver, H. A., et al. 2007, Natur, 448, 172
Dello Russo, N., Vervack, R. J., J., Lisse, C. M., et al. 2011, ApJL, 734, L8
Dello Russo, N., Vervack, R. J., J., Weaver, H. A., et al. 2008, ApJ, 680, 793
DiSanti, M. A., Anderson, W. M., Villanueva, G. L., et al. 2007, ApJ, 661, L101
DiSanti, M. A., Villanueva, G. L., Paganini, L., et al. 2014, Icar, 228, 167
Dodson-Robinson, S. E., Evans, N. J., I., Ramos, A., Yu, M., & Willacy, K. 2018, ApJL, 868, L37
Edwards, D. P. 1992, GENLN2: A general line-by-line atmospheric transmittance and radiance model, v3.0: Description and users guide, Zenodo, doi:10.5065/D6W37T86
Eistrup, C., Walsh, C., & van Dishoeck, E. F. 2016, A&A, 595, A83
Eistrup, C., Walsh, C., & van Dishoeck, E. F. 2018, A&A, 613, A14
Faggi, S., Mumma, M. J., Villanueva, G. L., Paganini, L., & Lippi, M. 2019, AJ, 158, 254
Feldman, P. D., Cochran, A. L., & Combi, M. R. 2004, in Comets II, ed. M. C. Festou, H. U. Keller, & H. A. Weaver (Tucson, AZ: Univ. Arizona Press), 425
Fink, U. 2009, Icar, 201, 311
Furuya, K., & Aikawa, Y. 2014, ApJ, 790, 97
Garaud, P., & Lin, D. N. C. 2007, ApJ, 654, 606
Garrod, R. T., & Herbst, E. 2006, A&A, 457, 927
Gelaro, R., McCarty, W., Suarez, M. J., et al. 2017, JCli, 30, 5419
Geppert, W. D., Hamberg, M., Thomas, R. D., et al. 2006, FaDi, 133, 177
Gibb, E. L., Bonev, B. P., Villanueva, G., et al. 2012, ApJ, 750, 102
Gibb, E. L., Mumma, M. J., Dello Russo, N., DiSanti, M. A., & Magee-Sauer, K. 2003, Icar, 165, 391
Gicquel, A., Milam, S. N., Coulson, I. M., et al. 2015, ApJ, 807, 19
Gomes, R., Levison, H. F., Tsiganis, K., & Morbidelli, A. 2005, Natur, 435, 466
Hidaka, H., Watanabe, N., Shiraki, T., Nagaoka, A., & Kouchi, A. 2004, ApJ, 614, 1124
Hiraoka, K., Takayama, T., Euchi, A., Handa, H., & Sato, T. 2000, ApJ, 532, 1029
Hiraoka, K., Wada, A., Kitagawa, H., et al. 2005, ApJ, 620, 542
Hoban, S., Mumma, M., Reuter, D. C., et al. 1991, Icar, 93, 122
Kama, M., Bruderer, S., van Dishoeck, E. F., et al. 2016, A&A, 592, A83
Kawakita, H., Kobayashi, H., Dello Russo, N., et al. 2013, Icar, 222, 723
Kobayashi, H., Bockelée-Morvan, D., Kawakita, H., et al. 2010, A&A, 509, A80
Kunde, V. R., & Maguire, W. C. 1974, JQSRT, 14, 803
Levison, H. F., Duncan, M. J., Brasser, R., & Kaufmann, D. E. 2010, Sci, 329, 187
Levison, H. F., & Morbidelli, A. 2003, Natur, 426, 419
Lippi, M., Villanueva, G. L., Mumma, M. J., et al. 2020, AJ, 159, 157
Magee-Sauer, K., Mumma, M. J., DiSanti, M. A., Russo, N. D., & Rettig, T. W. 1999, Icar, 142, 498
McLean, I. S., Becklin, E. E., Bendiksen, O., et al. 1998, Proc SPIE, 3354, 566
Meier, R., Eberhardt, P., Krankowsky, D., & Hodges, R. R. 1993, A&A, 277, 677
Mumma, M., Charnley, S., Cordiner, M., et al. 2019, EPSC-DPS Meeting, 2019, EPSC–DPS2019–1916
Mumma, M. J., Bonev, B. P., Villanueva, G. L., et al. 2011, ApJL, 734, L7
Mumma, M. J., Charnley, S., Cordiner, M., et al. 2018, AAS Meeting, 50, 209.02
Mumma, M. J., & Charnley, S. B. 2011, ARA&A, 49, 471
Mumma, M. J., Charnley, S. B., Cordiner, M., Paganini, L., & Villanueva, G. L. 2017, AAS Meeting, 49, 414.19
Mumma, M. J., Dello Russo, N., DiSanti, M. A., et al. 2001a, IAUC, 7578, 2
Mumma, M. J., DiSanti, M. A., Dello Russo, N., et al. 2003, AdSpR, 31, 2563
Mumma, M. J., DiSanti, M. A., Magee-Sauer, K., et al. 2005, Sci, 310, 270
Mumma, M. J., McLean, I. S., DiSanti, M. A., et al. 2001b, ApJ, 546, 1183
Mumma, M. J., Weaver, H. A., Larson, H. P., Davis, D. S., & Williams, M. 1986, Sci, 232, 1523
Oka, A., Nakamoto, T., & Ida, S. 2011, ApJ, 738, 141
Paganini, L., Mumma, M. J., Bonev, B. P., et al. 2012, Icar, 218, 644
Paganini, L., Mumma, M. J., Villanueva, G. L., et al. 2014, ApJ, 791, 122

Piso, A.-M. A., Öberg, K. I., Birnstiel, T., & Murray-Clay, R. A. 2015, ApJ, 815, 109
Poch, O., Istiqomah, I., Quirico, E., et al. 2020, Sci, 367, aaw7462
Pontoppidan, K. M., Salyk, C., Banzatti, A., et al. 2019, ApJ, 874, 92
Qasim, D., Chuang, K. J., Fedoseev, G., et al. 2018, A&A, 612, A83
Radeva, Y. L., Mumma, M. J., Bonev, B. P., et al. 2010, Icar, 206, 764
Radeva, Y. L., Mumma, M. J., Villanueva, G. L., et al. 2013, Icar, 223, 298
Rothman, L. S., Gamache, R. R., Tipping, R. H., et al. 1992, JQSRT, 48, 469
Rothman, L. S., Jacquemart, D., Barbe, A., et al. 2005, JQSRT, 96, 139
Ruaud, M., & Gorti, U. 2019, ApJ, 885, 146
Schwarz, K. R., & Bergin, E. A. 2014, ApJ, 797, 113
Schwarz, K. R., Bergin, E. A., Cleeves, L. I., et al. 2018, ApJ, 856, 85
Tielens, A. G. G. M. 2013, RvMP, 85, 1021
Villanueva, G. L., Bonev, B. P., Mumma, M. J., et al. 2006, ApJ, 650, L87
Villanueva, G., Magee-Sauer, K., & Mumma, M. 2013, JQSRT, 129, 158
Villanueva, G. L., DiSanti, M. A., Mumma, M. J., & Xu, L. H. 2012a, ApJ, 747, 37
Villanueva, G. L., Mumma, M. J., Bonev, B. P., et al. 2012b, JQSRT, 113, 202
Villanueva, G. L., Mumma, M. J., DiSanti, M. A., et al. 2011a, Icar, 216, 227
Villanueva, G. L., Mumma, M. J., & Magee-Sauer, K. 2011b, JGRE, 116, E08012
Villanueva, G. L., Mumma, M. J., Novak, R. E., & Hewagama, T. 2008, Icar, 195, 34
Villanueva, G. L., Smith, M. D., Protopapa, S., Faggi, S., & Mandell, A. M. 2018, JQSRT, 217, 86
Walsh, C., Millar, T. J., & Nomura, H. 2010, ApJ, 722, 1607
Walsh, C., Nomura, H., & van Dishoeck, E. 2015, A&A, 582, A88
Weaver, H. A., Feldman, P. D., A'Hearn, M. F., Dello Russo, N., & Stern, S. A. 2011, ApJL, 734, L5
Wei, C.-E., Nomura, H., Lee, J.-E., et al. 2019, ApJ, 870, 129
Young, J. 2007, IAUC, 8857, 1